REPUBLIC OF TÜRKİYE
ADANA ALPARSLAN TÜRKEŞ SCIENCE AND TECHNOLOGY UNIVERSITY

GRADUATE SCHOOL
ELECTRICAL AND ELECTRONIC ENGINEERING DEPARTMENT

SENSORLESS BRUSHLESS DC MOTOR DRIVE DESIGN AND PERFORMANCE COMPARISON OF DIFFERENT CONTROL METHODS

EMRE YORAT

M.Sc.

ADANA 2022

REPUBLIC OF TÜRKİYE
ADANA ALPARSLAN TÜRKEŞ SCIENCE AND TECHNOLOGY UNIVERSITY

GRADUATE SCHOOL
ELECTRICAL AND ELECTRONIC ENGINEERING DEPARTMENT

SENSORLESS BRUSHLESS DC MOTOR DRIVE DESIGN AND PERFORMANCE COMPARISON OF DIFFERENT CONTROL METHODS

EMRE YORAT

M.Sc.

THESIS ADVISOR
ASSOC. PROF. DR. LÜTFÜ SARIBULUT

SECOND ADVISOR
ASST. PROF. DR. NECDET SİNAN ÖZBEK

ADANA, 2022

DECLARATION OF CONFORMITY

In this thesis study, which was prepared following the thesis writing rules of Adana Alparslan Türkeş Science and Technology University Institute of Graduate School, I declare that I provide all the information, documents, evaluations and results in accordance with scientific ethics and moral codes without resorting to any means or assistance that would be contrary to scientific ethics and traditions. I also declare that I refer to all of the articles I used in this study with appropriate references and accept all moral and legal consequences if a situation is found contrary to my statement regarding my work.

15/12/2022

[İmza]

Emre YORAT

ÖZET

SENSÖRSÜZ FIRÇASIZ DA MOTOR SÜRÜCÜ TASARIMI VE FARKLI KONTROL YÖNTEMLERİNİN PERFORMANS KARŞILAŞTIRMASI

Emre YORAT
Yüksek Lisans, Elektrik-Elektronik Anabilim Dalı
Danışman: Doç. Dr. Lütfü SARIBULUT
II. Danışman: Dr. Öğr. Üyesi Necdet Sinan ÖZBEK
Aralık 2022, 48 sayfa

Fırçasız doğru akım motorları (FDAM) yüksek verimlilikleri, yüksek tork/ağırlık oranları, az bakım gerektirmeleri vb. özelliklere sahip olmaları sebebiyle elektrikli ev aletleri, robotik ve elektrikli araçlar gibi birçok uygulama alanında tercih edilmektedir. Bu motorların çalıştırılmaları için elektronik sürücü ve kontrol kartına ihtiyaç duyulur. Bu çalışmada FDAM için L298N H-köprü evireç yapısı ve Atmel mikrodenetleyici ile düşük maliyetli sürücü devresi tasarlanmış ve sensörsüz kontrol algoritması önerilmiştir. Ayrıca 120°, 150° ve 180° komütasyon, doğrudan sayısal sentezleme (DSS) tabanlı sinüzoidal kontrol ve ters-EMK'ya dayalı kontrol yöntemleri benzetim ve deneysel çalışmalarda uygulanmıştır. Yöntemlerin performans karşılaştırması güç kaynağından çekilen akım, dakikadaki devir sayısı ve ağırlık kaldırma kuvveti değerleri açısından gerçekleştirilmiştir. Önerilen yöntemin performansı, uygulanan diğer kontrol yöntemleri içerisinde dikkat çeken sonuçları olan bir yöntemle karşılaştırılarak değerlendirilmiştir. Elde edilen verilere göre, önerilen yöntemle karşılaştırılan yöntemden daha iyi sonuçlara ulaşılmıştır.

Anahtar Kelimeler: FDAM, DSS, Kontrol, Sinüzoidal Kontrol, Deneysel Uygulama

ABSTRACT

SENSORLESS BRUSHLESS DC MOTOR DRIVE DESIGN AND PERFORMANCE COMPARISON OF DIFFERENT CONTROL METHODS

Emre YORAT
M.Sc., Department of Electrical and Electronic Engineering
Supervisor: Assoc. Prof. Dr. Lütfü SARIBULUT
Co-Supervisor: Asst. Prof. Dr. Necdet Sinan ÖZBEK
December 2022, 48 pages

Brushless direct current motors (BLDCMs) have been preferred in many application areas such as household appliances, robotics, and electric vehicles for having high efficiency, high torque-to-weight ratio, demanding less maintenance and so on. Electronic driver and control card are needed to operate these motors. In this study, a low-cost drive circuit is designed for BLDCMs with L298N H-bridge inverter structure and Atmel microcontroller and a sensorless control algorithm is proposed. In addition, 120°, 150°, and 180° commutation, direct digital synthesis (DDS) based sinusoidal control, and back-EMF-based control methods are applied in simulation and experimental studies. The performance benchmarking of the methods is realized in terms of values of current drawn from the power supply, revolution per minute, and thrust. The performance of the proposed method is evaluated by comparing it with a method having remarkable results within other applied control methods. According to the acquired data, better results are achieved with the proposed method than the compared method.

Keywords: BLDCM, DDS, Control, Sinusoidal Control, Experimental Application

Dedication

To my parents…

ACKNOWLEDGMENTS

I would like to thank my supervisor Assoc. Prof. Dr. Lütfü SARIBULUT for involving me work in this subject and helping me in every detail of the thesis. I am also grateful to my co-supervisor Asst. Prof. Dr. Necdet Sinan ÖZBEK for showing me right directions to focus on and generous support. Without their guidance this thesis would not have existed.

I would also like to thank Prof. Dr. Ahmet TEKE, Asst. Prof. Dr. Özgür ÇELİK, and Asst. Prof. Dr. Kasım ZOR for accepting to be a member of the examining committee for my thesis. My sincere thanks to Asst. Prof. Dr. Kasım ZOR and Asst. Prof. Dr. Özgür ÇELİK for their unconditional helps.

I would also like to express my gratitude to my parents and brother.

This thesis was financially supported by the Scientific Research Unit of Adana Alparslan Türkeş Science and Technology University with project number 21303007.

TABLE OF CONTENTS

LIST OF FIGURES

LIST OF TABLES

NOMENCLATURE

AI	: Artificial Intelligence
ADC	: Analog to Digital Conversion
BDCM	: Brushed Direct Current Motor
BLDCM	: Brushless Direct Current Motor
DAC	: Digital to Analog Converter
DDS	: Direct Digital Synthesis
FOC	: Field Oriented Control
IGBT	: Insulated Gate Bipolar Transistor
IM	: Induction Motor
MOSFET	: Metal Oxide Semiconductor Field Effect Transistor
PCB	: Printed Circuit Board
PI	: Proportional Integral
PMSM	: Permanent Magnet Synchronous Motor
PWM	: Pulse Width Modulation
RPM	: Revolutions per Minute
SPWM	: Sinusoidal Pulse Width Modulation
SVPWM	: Space Vector Pulse Width Modulation

SYMBOLS

u_a, u_b, u_c	: Stator Phase Voltages (V)
R_a, R_b, R_c, R	: Stator Phase Resistances (Ω)
i_a, i_b, i_c	: Stator Phase Currents (A)
L_{ab}, L_{bc}, L_{ca}, M	: Stator Phase Inductances (L)
e_a, e_b, e_c	: Back Electromotive Forces (V)
K_e	: Back Electromotive Force Constant (Wb)
T_e	: Electromagnetic Torque (Nm)
P	: Power (Watts)
ω	: Angular Velocity (rad/s)
θ	: Position angle (rad)

1. INTRODUCTION

Brushless Direct Current Motors (BLDCMs) have been widely used in various fields like household appliances, drones, automobile industry, robotics, and aerospace applications due to their high efficiency, compact size, high dynamic response, controllability, and reliability. It is a synchronous electric machine that rotor and stator magnetic fields synchronously follow each other. The rotor and stator of a BLDCM include permanent magnets and windings, respectively. Rotating stator magnetic field is obtained by energizing stator windings by following a commutation sequence. Mostly, three-phase inverter circuits are used to energize windings. Application of the sequence is depended on the rotor position since the interaction of the stator and rotor magnetic fields generates torque that is related to the angle between these two fields. Therefore, the positional information of the rotor is necessary to commutate stator windings correctly. Thus, a means of acquiring the rotor position information is essential. One method for detecting the rotor position even at standstill is by placing hall-effect sensors on the stator but these sensors affect system cost, size, and reliability in a negative way (Cheng & Tzou, 2003; Gamazo-Real, Vázquez-Sánchez, & Gómez-Gil, 2010).

As a result, sensorless control has gained more attention from researchers and many techniques have been developed to detect the rotor position with various approaches such as direct detection of back electromotive force (back-EMF), estimation of back-EMF by using observer theory, artificial intelligence, flux-linkage, inductance variation. Generally, these techniques are coupled with controller(s) and a commutation method mainly, 120°, 150°, and 180° commutation, space vector pulse width modulation (SVPWM), and sinusoidal pulse width modulation (SPWM).

Selection of an efficient commutation method is crucial where a battery is used as the power source. In this thesis, numerous commutation methods have been tested on a drone motor for evaluating low-high speed performance. In this context, 120°, 150°, and 180° commutation, and a direct digital synthesis (DDS) based sinusoidal commutation method is applied in simulation and experimental studies. Special attention has been given to 120° commutation by applying it on back-EMF-based control since it is one of the popular techniques to drive BLDCM. Speed, thrust, current drawn, and waveforms of each method are given.

The principal contributions of this thesis are as follows:

- The performance comparison of the aforementioned four methods, which have not been addressed yet in the literature, have been conducted experimentally on a BLDCM with a low-cost standalone drive system.
- It is the first time that the comparison of the DDS algorithm based sinusoidal PWM method with widely used commutation methods for BLDC motor control was realized.
- The performance of the proposed back-EMF-based three-step method is evaluated in this research.

The rest of the study is summarized as follows. Section 2 details the sensorless control methods of BLDCMs by dividing them into rotor position sensing and commutation methods. Section 3 describes the building blocks of a BLDCM and its operating principles. Also, a low-cost inverter circuit design and the other components of the drive system are presented. In section 4, simulation and experimental studies of the commutation methods are realized, and the proposed three-step commutation method is explained. Performance results are discussed in section 5. The study is ended with some concluding remarks given in the last section.

2. LITERATURE REVIEW

Control of BLDCM is a wide topic that has been investigated by many researchers in the field. BLDCMs do not have physical commutation mechanisms such as a commutator and brushes. Therefore control procedure for BLDCM is more complex than the brushed direct current motor (BDCM) since it requires information of the rotor position (Mousmi, Abbou, & El Houm, 2017). In the literature, sensored and sensorless control methods have been used and improved to obtain the rotor position. However, A BLDCM control system not only acquires the rotor position, it also implements a commutation method on inverter side mainly 120°, 150°, and 180° commutation, SVPWM, and sinusoidal pulse width modulation (SPWM) and can include blocks such as torque and speed controllers which meets the speed and torque requirements of the application.

The sensored control methods usually use hall-effect sensors mounted on the stator displaced 120 electrical degrees from one another and parallel to the rotor permanent magnets' (Al-Adsani, Alsharidah, & Beik, 2021) as shown in Figure 2.1 to obtain position signals, while sensorless BLDCMs acquire the rotor position information by using various principles. In the literature review section, widely used rotor position detection methods, initial rotor position sensing techniques, starting strategies, commutation methods, and control topologies of sensorless BLDCMs are presented (Xia, 2012).

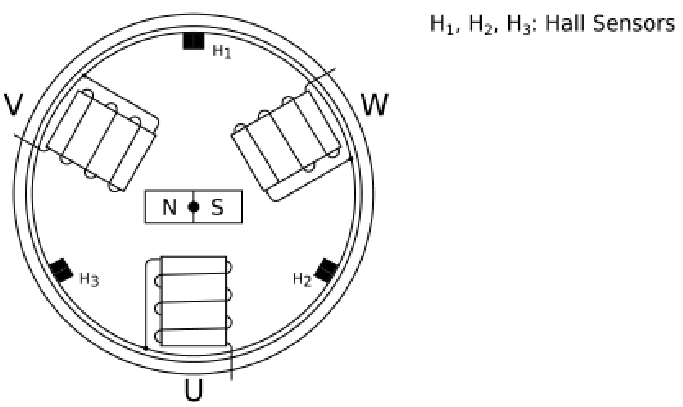

Figure 2.1. Hall-effect sensors are illustrated on a BLDCM stator (Fonseca, Nielsen, & Both, 2011)

2.1. Sensorless BLDCM Rotor Position Sensing Methods

Many rotor position sensing methods have been developed by researchers it is seen that more attention has been given to back-EMF-based methods. Typically, these methods detect the rotor position only within a certain speed range. Also, the flux-linkage and artificial-intelligence-based methods are used to detect position information. However, most of position sensing methods can be implemented only in certain speed range. Therefore, more than one methods can be integrated to achieve full-speed operation. In this part of the thesis, commonly used methods for rotor position sensing are summarized.

2.1.1. Back-EMF-Based Position Sensing

The back-EMF-based position detection methods are the most popular sensorless control method and it is generally implemented for medium-high speed range operation (Li, Wu, Xu, Sun, & Zhao, 2021) because the magnitude of back-EMF is dependent upon the rotor speed and it is undetectable at low speeds (Khambhadiya & Dhaneria, 2021). In this subsection, the operation of commonly used back-EMF-based rotor position detection methods is explained. Typically, these methods try to compensate for other methods' defective sides. The working principles of these methods are given below.

In the terminal voltage sensing method, the sensorless operation is obtained by detecting zero-crossing of the back-EMFs of nonexcited phase windings and shifting them 30 electrical degrees to acquire six separate rotor position signals also known as commutation instants. The commutation instants and the zero-crossing points of each phase back-EMF waveforms are given in Figure 2.2 (Iizuka, Uzuhashi, Kano, Endo, & Mohri, 1985; Xia, 2012).

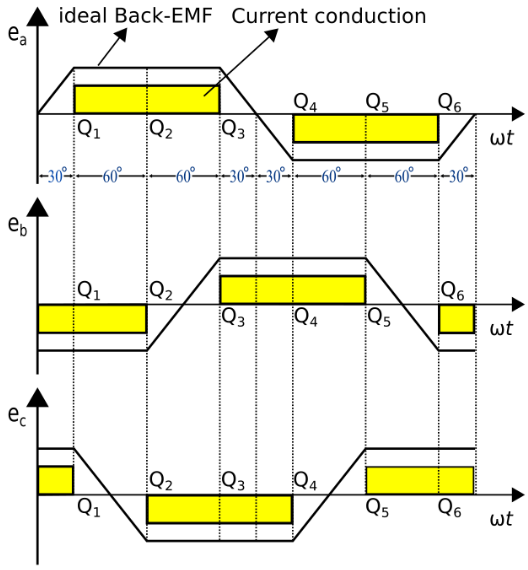

Figure 2.2. Illustration of phase back-EMFs and current conduction.

In the third-harmonic back-EMF method, the phase voltages are summed and integrated to get the third-harmonic flux linkage which the zero crossing of this signal is exactly the commutation instant of the BLDC motor (Moreira, 1996; Yang, Zhu, Bin, Zhang, & Gong, 2021). An illustration of the third-harmonic-based back-EMF method is given in Figure 2.3.

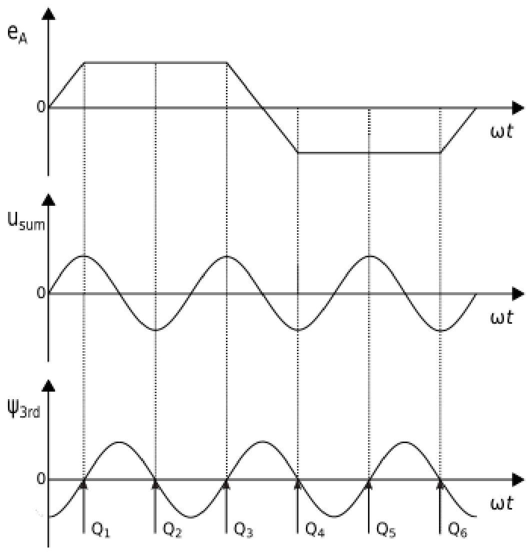

Figure 2.3. Relationship between the back-EMF and third harmonic signal (Xia, 2012).

In the back-EMF integration method, the unenergized phase back-EMF is integrated and compared with a determined threshold value (Attar, Bouchnaif, & Grari, 2021). The commutation instant is when the integral value is equal to the threshold. The commutation instants of applied integration method are illustrated in Figure 2.4 (Becerra, RC., Jahns, TM., Ehsani, 1991).

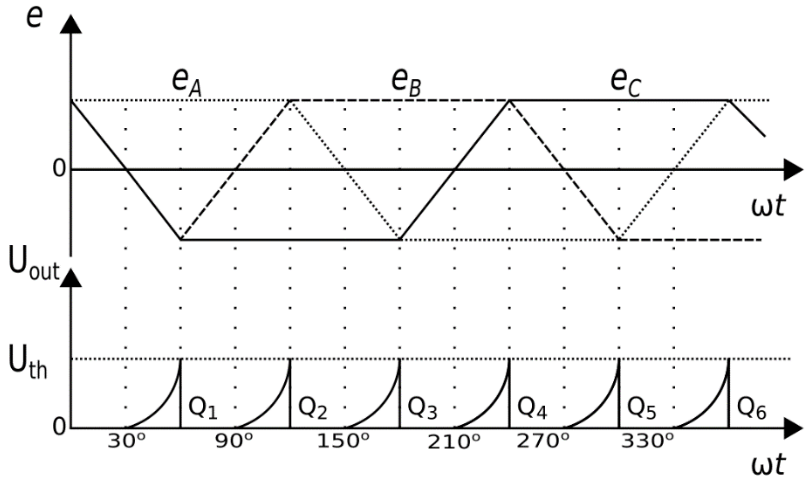

Figure 2.4. The relationship between phase back-EMFs and commutation points by the integration method (Xia, 2012).

In the freewheeling diode method, the zero-crossing points of the back-EMF are found by the conduction state of the freewheeling diodes. During the off parts of the PWM modulation, the current flows through from the freewheeling diodes. After proving the validity of the method with circuit analyses, the rotor position is detected by placing comparator circuits on each of the freewheeling diodes (Gamazo-Real et al., 2010; Ogasawara & Akagi, 1991).

In the line back-EMF method, the line back-EMF voltages are measured, and detected zero crossing points of this signal are used as commutation instants without processing for angles as mentioned in the terminal voltage sensing method (Xia, 2012; Johnson, Ehsani, & Guzelgunler, 1999). The commutation points of the applied line back-EMF method are illustrated in Figure 2.5. In addition, the line back-EMF difference method is also used to control BLDCM (Ding & Liu, 2022).

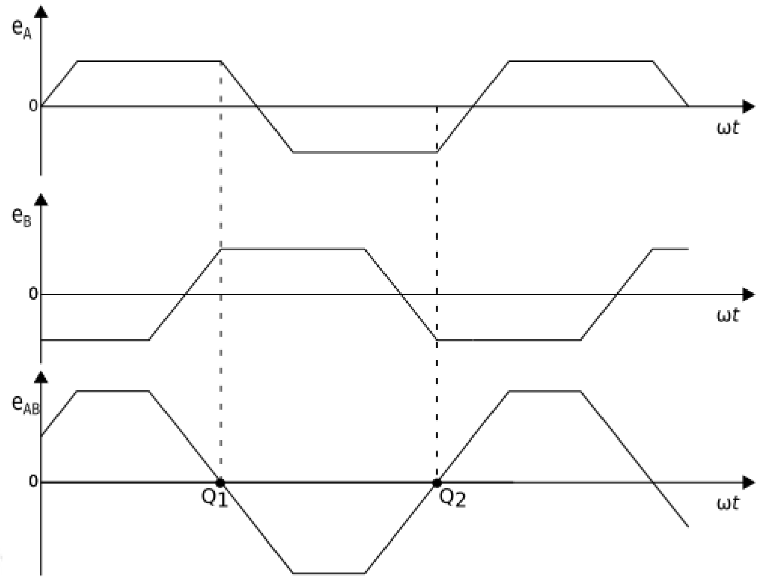

Figure 2.5. The derivation of commutation points for the line back-EMF method is illustrated (Xia, 2012).

2.1.2. Observer-Based Position Sensing

Observer-based methods use computational techniques on the mathematical model of BLDCM to estimate the back-EMF signal. One of the advantages is that back-EMF can be estimated even at low speeds which is a shortcoming of conventional back-EMF detection methods. (Saha & Singh, 2021). There are various types of observer methods used in the control of BLDCM, such as Kalman filter, nonlinear observer (Shouse & Taylor, 1998), full order (Consoli, Musumeci, Testa, & Raciti, 1994), disturbance (Senjyu & Uezato, 1995), reduced-order (Kim & Sul, 1995; Solsona, Valla, & Muravchik, 1996), and sliding-mode (Y. S. Kim, Ahn, You, & Cho, 1996) observer. A control scheme of sliding-mode observer is given in Figure 2.6. In current control theories, a state feedback controller and state observer can be integrated to create a controller architecture. The design of a closed-loop system and the overall system performance enhancement are addressed by this method. The state variables are required for the creation of a state feedback controller but, some of these state variables cannot be measured in practice. In order to address this issue, the state observation or state reconstruction are proposed (Xia, 2012).

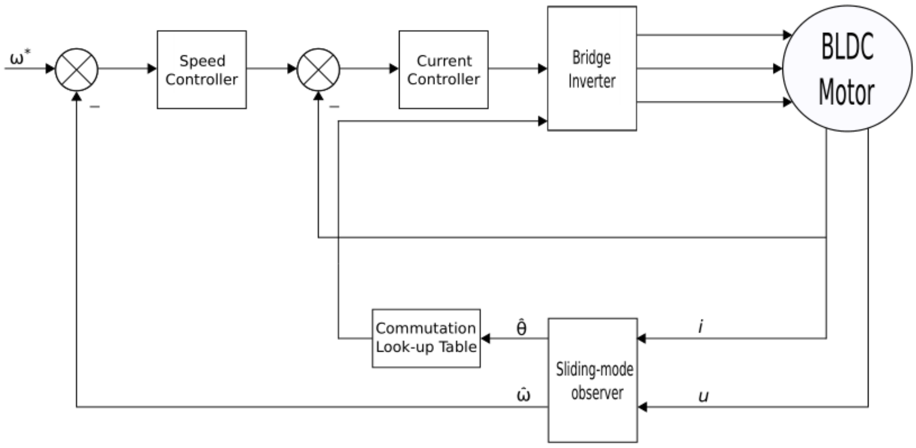

Figure 2.6. An example for observer-based rotor position sensing (Xia, 2012).

2.1.3. Flux-linkage-Based Position Sensing

The rotor position is estimated by applying polynomial curve fitting to the flux linkage. The flux linkage is calculated by taking the integral of measured voltages and currents. This is expressed in the voltage equation of the motor where V, i, R, and λ denote the input voltage, the current, the resistance, and the flux linkage, respectively, as shown below (Kim, T., Lee, H.W., Ehsani & Ehsani, 2007).

$$V = Ri + \frac{d}{dt}\lambda \tag{2.1}$$

$$\lambda = \int_0^t (V - Ri)dt \tag{2.2}$$

2.1.4. Intelligence-Based Position Sensing

In this position sensing method, the rotor position information is detected using a built relationship between the voltage, current, and rotor position with the artificial intelligence (AI) based theories. Then, the commutation signals are generated by a controller using the established relationship. One of the advantages of intelligence-based algorithms is it does not need the precise mathematical model of the motor. Therefore, it could be the preferred control method where nonlinearities exist in the model such as in BLDCM. (Wang et al., 2022). To sum up, AI based BLCDM rotor position detection system has strong robustness against disturbance factors that exist in the motor (Xia, 2012). Illustration of AI based position sensing method is given in Figure 2.7.

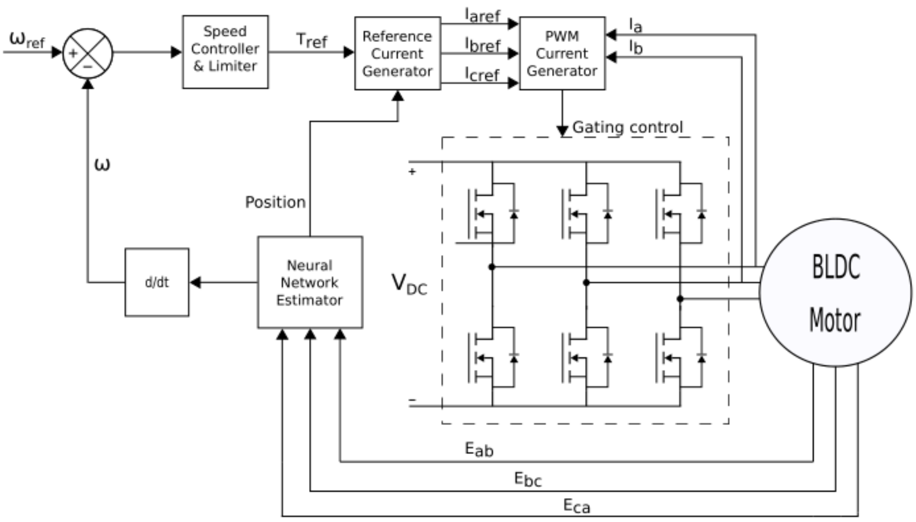

Figure 2.7. Neural network estimator-based control (Kumar & Padmanaban, 2006)

2.2. Starting and Sensorless Control of BLDCM

The rotor position is found by analyzing induced back-EMF at the stator windings by the back-EMF-based commutation methods. However, detection of the rotor position is difficult at low speeds. Because the amplitude of back-EMF is proportional to the rotor speed. Therefore one of the problems associated with sensorless BLDCM control becomes the starting of the motor. BLDCM can be run by applying arbitrary voltage vectors at the start. The disadvantage is that it can result in a high starting current, insufficient torque, start-up failures, backward rotation, etc (Champa, Somsiri, Wipasuramonton, & Nakmahachalasint, 2009; Lee, Kim, Kim, & Kwon, 2008). Thus, robust starting and initial rotor position detection techniques are needed and many researchers have studied this subject and developed methods in this regard. Next section discusses commonly used sensorless BLDCMs starting methods.

2.2.1. Voltage/frequency Scalar Control

In voltage/frequency (V/F) control of BLDCM, the speed of the motor adjusted with the applied voltage and frequency. The principle of this method is that the ratio of the stator voltage and frequency is held constant which ensures a constant stator magnetic flux (Strobl, n.d.). The method is simple to implement, and no measurement of current or speed is needed (Jani, n.d.). Figure 2.8 illustrates V/F scalar control.

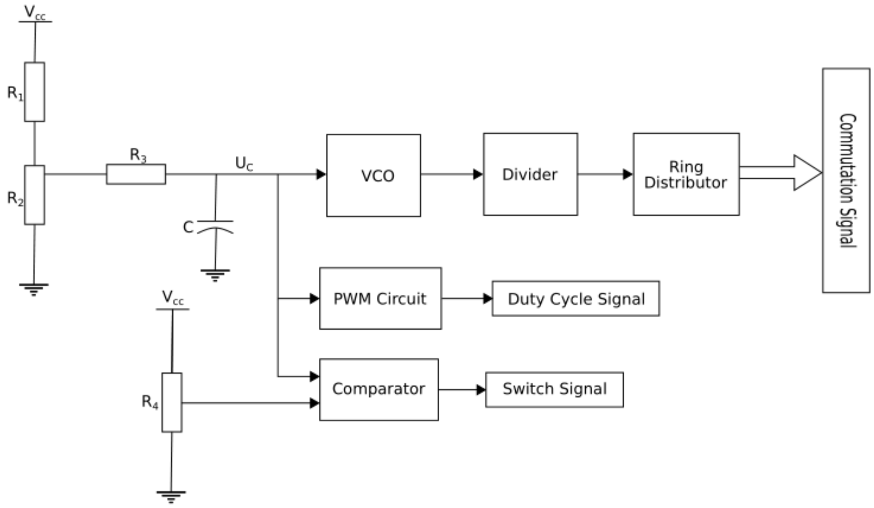

Figure 2.8. V/F control scheme (Xia, 2012)

2.2.2. The Presetting Method

In this method, two stator phase windings are excited for a preset time to align the rotor with the resultant force vector as shown in the Figure 2.9. After locating the rotor, the motor can be accelerated with a chosen control method. Benefits of the presetting startup method are simple execution and stable startup. It can guarantee that the motor starts at a standstill and transitions properly to the sensorless control regardless of the initial rotor position (Xia, 2012).

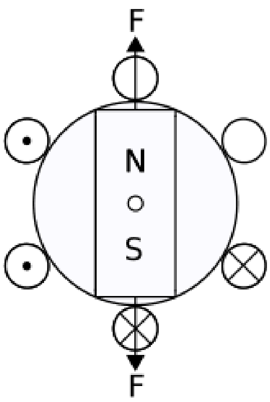

Figure 2.9. The presetting method illustration (Ogasawara & Akagi, 1991)

2.2.3. Inductance Variation-Based Rotor Position Sensing

The inductance variation-based position sensing method uses the magnetic saturation phenomenon of the stator core to detect the initial rotor position (Jang, Park, & Chang, 2002).

The magnetization of the stator core close to the rotor permanent magnet is higher. Thus, when a voltage vector is applied to that stator winding, the rate of change of current will be large with respect to another applied voltage signal in the opposite direction (Lee & Sul, 2006). Aforementioned principle is used as follows. Voltage vectors are applied at a constant time period and resulting current magnitudes are compared. By this method, the rotor position can be deduced with a resolution of at least 60° (Zhou, Li, Chen, & Shi, 2021).

2.2.4. Field-Oriented Control

Field-Oriented Control (FOC) is a very efficient control method that can be used in BLDCM, permanent magnet synchronous motor (PMSM), and induction motors (IC). FOC aims to control the magnetic flux and the torque by regulating the d and q components of the stator currents or relative fluxes (Bayır, 2019). FOC is a closed-loop control algorithm that operates on the stator voltages and currents. In this method, the stator currents i_a, i_b and i_c are transformed to i_α and i_β currents by using the Clarke Transform. The feedback signal 'speed' is subtracted from the reference value. Then, the error signal is used in the Proportional integral (PI) controller to obtain the desired I_{qref} value.

Since PI controllers can work on DC quantities, Park transform is used to convert the two-axis stationary reference frame quantities to the rotating reference frame quantities. After applying the Park Transform, I_d and I_q quantities are used in PI controllers to generate the control signals V_d and V_q based on I_{qref}, I_{dref}, I_d, and I_q values. Afterward, the inverse Park and Clarke transformations are applied to get the three-phase voltage signals V_a, V_b, and V_c which provide the duty cycles of the Pulse-width modulation (PWM) channels (O'Rourke, Qasim, Overlin, & Kirtley, 2019). Implementation details of the technique are shown in Figure 2.10.

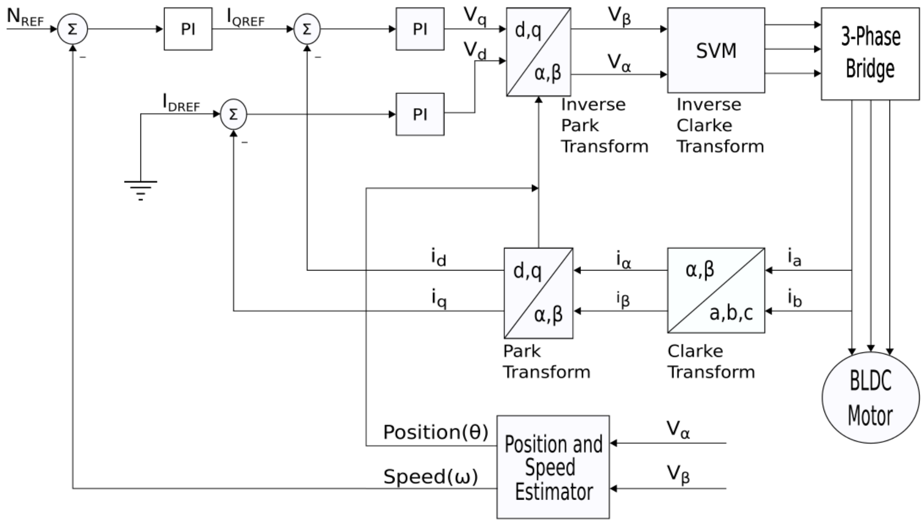

Figure 2.10. Field-oriented control scheme

2.3. BLDCM Commutation Methods

BLDCMs are rotated by changing the direction of current in the phase windings in accordance with the rotor position. Changing the direction of the current (changing the energized phases) is called as commutation. The commutation is realized according to the rotor position. The rotor position defines which commutation state is to be applied to the windings. The commutation action is carried out by an inverter circuit such us given in Figure 2.11. The inverter circuit has switching elements that turn on and off depending on the gate signals. Commutation methods are responsible for generating gate signals. There are different commutation methods in the literature for example 120°, 150°, and 180° commutation, sinusoidal PWM, and SVPWM are the most commonly used ones. Each method has advantages and disadvantages with respect to complexity or other performance parameters.

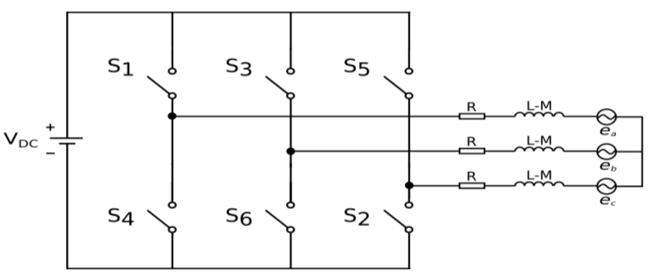

Figure 2.11. BLDCM model and connection to a representative inverter circuit.

2.3.1. 120° Commutation Method

This method is also called as trapezoidal or six-step control. Switching sequence of the method and application on a typical inverter circuit is given by considering for first two steps in Figure 2.12 a), and Figure 2.12 b), respectively. In this method, the duration of each commutation state is 60 electrical degrees and there is a total of six commutation states. All switching elements conduct current for 120 electrical degrees as can be verified from the Figure 2.13. Continuous rotation of the motor is ensured by six commutation states that are applied to the motor recursively. The method has the advantage for sensorless control since it energizes two phase windings and leaves third winding unenergized. This gives the capability to measure the back-EMF on the unenergized phase to detect the rotor position which in turn can be used to switch to the next commutation state.

Step	S1	S4	S3	S6	S5	S2
1	1	0	0	1	0	0
2	1	0	0	0	0	1
3	0	0	1	0	0	1
4	0	1	1	0	0	0
5	0	1	0	0	1	0
6	0	0	0	1	1	0

(a)

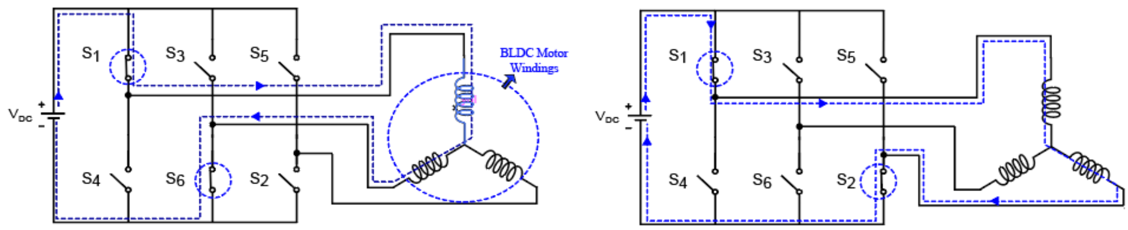

(b)

Figure 2.12. a) 120° commutation states b) Illustration of first two steps of above commutation states.

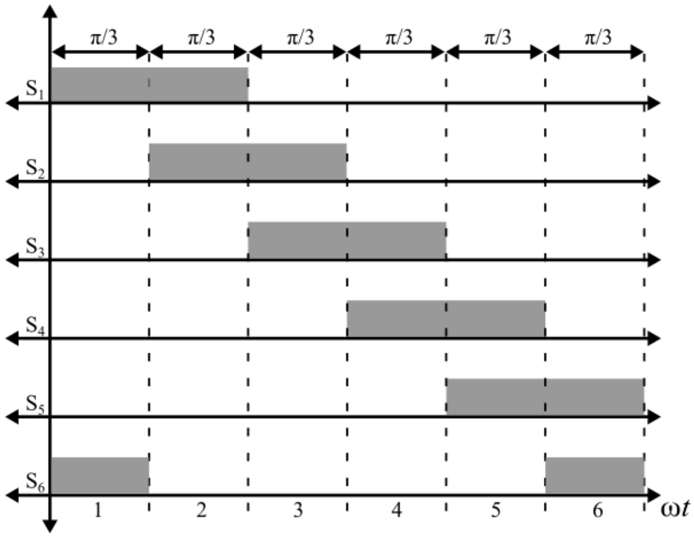

Figure 2.13. Current conduction of switches for 120° commutation

2.3.2. 150° Commutation Method

The 150° commutation method is also called as twelve-step commutation. The duration of each commutation state is 30 electrical degrees and the number of active switches is two or three. The switching sequence of the method and application on a typical inverter circuit for the first three steps are given in Figure 2.14 a), and Figure 2.14 b), respectively. The method consists of twelve commutation states and all switching elements in the inverter circuit conduct current for 150 electrical degrees. It can be verified from Figure 2.15. The method has advantages over 120° and 180° commutation methods such as increased RMS values of the output voltages, a 30° safety margin period to avoid the short circuit on dc supply (Saied, Mostafa, Abdel-Moneim, & Yousef, 2006).

Step	S1	S4	S3	S6	S5	S2
1	1	0	1	0	0	1
2	0	0	1	0	0	1
3	0	1	1	0	0	1
4	0	1	1	0	0	0
5	0	1	1	0	1	0
6	0	1	0	0	1	0
7	0	1	0	1	1	0
8	0	0	0	1	1	0
9	1	0	0	1	1	0
10	1	0	0	1	0	0
11	1	0	0	1	0	1
12	1	0	0	0	0	1

(a)

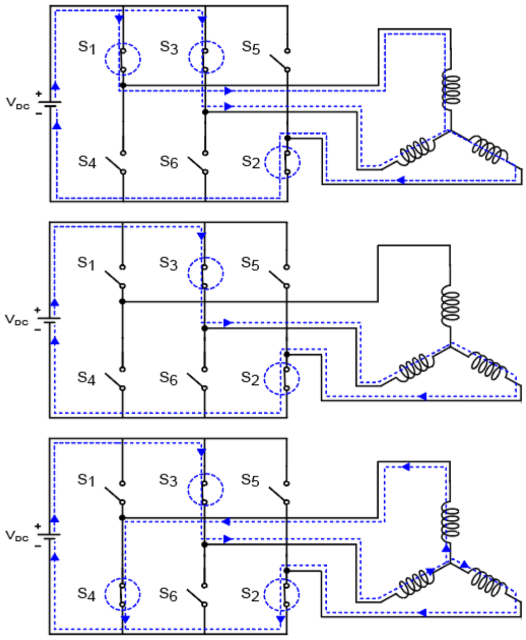

(b)

Figure 2.14. a) 150° commutation states b) Illustration of first three steps of above commutation states.

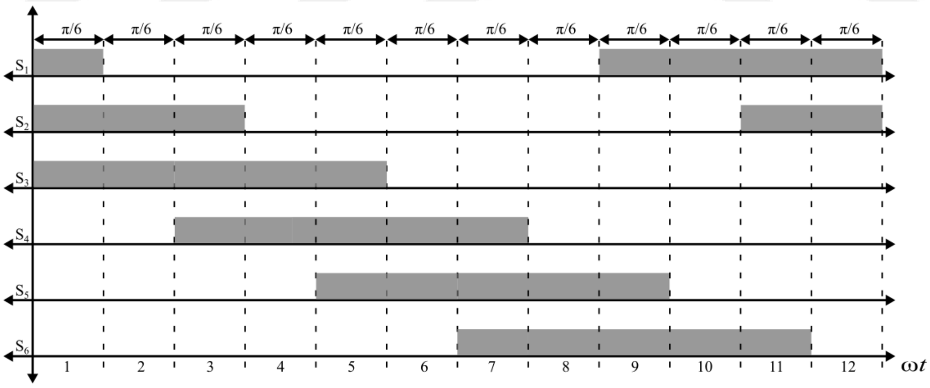

Figure 2.15. Current conduction of switches for 150° commutation

2.3.3. 180° Commutation Method

The switching sequence of the method and application on a typical inverter circuit is given for the first two steps in Figure 2.16 a), and Figure 2.16 b), respectively. The commutation method has six commutation states where each last for 60 electrical degrees. Three switching element is always active at every commutation step and each switching elements conducts current for 180 electrical degrees. It can be checked from Figure 2.17.

Step	S1	S4	S3	S6	S5	S2
1	1	0	1	0	0	1
2	0	1	1	0	0	1
3	0	1	1	0	1	0
4	0	1	0	1	1	0
5	1	0	0	1	1	0
6	1	0	0	1	0	1

(a)

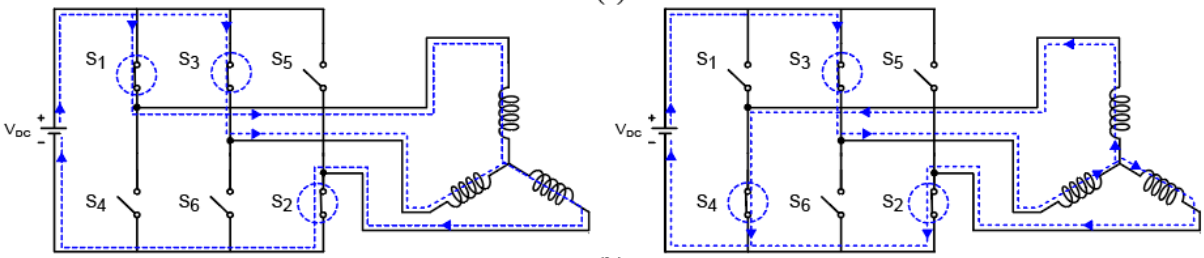

(b)

Figure 2.16. a) 180° commutation steps b) Illustration of first two steps of above commutation steps.

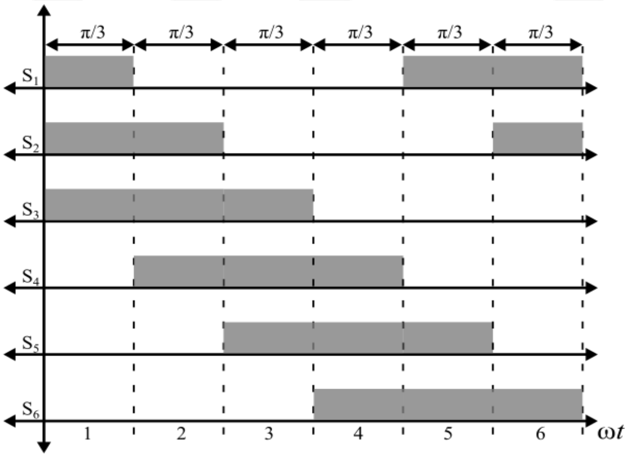

Figure 2.17. Current conduction of switches for 180° commutation

2.3.4. Space Vector PWM Method

Space vector PWM (SVPWM) is used to generate sine waves at each motor phase by turning on and off switching elements at specific time durations. For example, to synthesize voltage vector $\vec{U}$ that is shown in Figure 2.18, first $\vec{U}$ is decomposed to $\vec{U}_\alpha$ and $\vec{U}_\beta$ vectors with the transformation matrix given in Equation 3. $\vec{U}_\alpha$ and $\vec{U}_\beta$ correspond to inverter switching states S_1 and S_2 respectively. The time durations of the switching states are calculated by Equation 4. T_s is the total time to generate $\vec{U}$. it is also known as the fundamental period (Saribulut, Teke, & Tümay, 2012). The time shares of t_1 and t_2 are the durations to obtain $\vec{U}_\alpha$ and $\vec{U}_\beta$ vectors, respectively and rest of the time –t_0 and t_7- are filled with vectors $\vec{U}_0$ and $\vec{U}_7$. $\vec{U}_0$ and $\vec{U}_7$ represents inactive inverter states in which no voltage is applied to the phases (Montero, Vogelsberger, Ertl, & Wolbank, 2019).

$$\begin{pmatrix} \vec{U}_\alpha \\ \vec{U}_\beta \\ \vec{U}_0 \end{pmatrix} = \frac{2}{3} \begin{pmatrix} 1 & -\frac{1}{2} & -\frac{1}{2} \\ 0 & \frac{\sqrt{3}}{2} & -\frac{\sqrt{3}}{2} \\ \frac{1}{2} & \frac{1}{2} & \frac{1}{2} \end{pmatrix} \begin{pmatrix} \vec{U}_a \\ \vec{U}_b \\ \vec{U}_c \end{pmatrix} \tag{2.3}$$

$$\vec{U}(t) = \frac{t_0}{T_s}\vec{U}_0 + \frac{t_1}{T_s}\vec{U}_1 + \frac{t_2}{T_s}\vec{U}_2 + \frac{t_7}{T_s}\vec{U}_7 \tag{2.4}$$

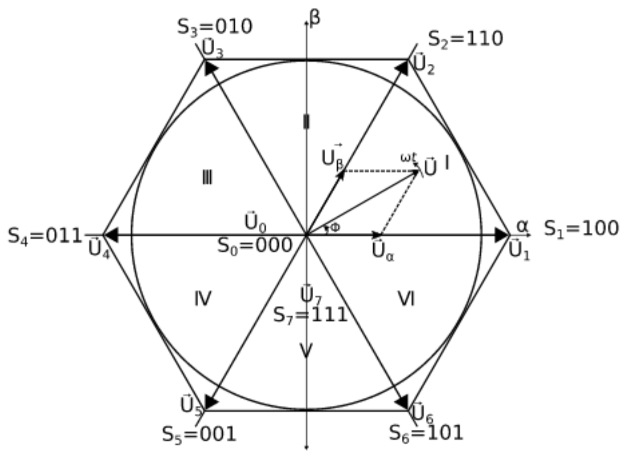

Figure 2.18. Space vector diagram (Saribulut et al., 2012)

2.3.5. Sinusoidal PWM Method

A practical and widely used modulation method for inverter and motor control applications is sinusoidal PWM. The principle operation of the method is that the modulating and the carrier signal are compared to generate PWM with varying duty cycles. The desired signal output is a sinusoidal wave thus a sinusoidal wave with the desired amplitude and frequency is used as modulating signal. The carrier signal is a triangular wave with a higher frequency (Gujjar & Kumar, 2017; Uslu, 2012). The generation of the sinusoidal waveform with the SPWM method is depicted in Figure 2.19.

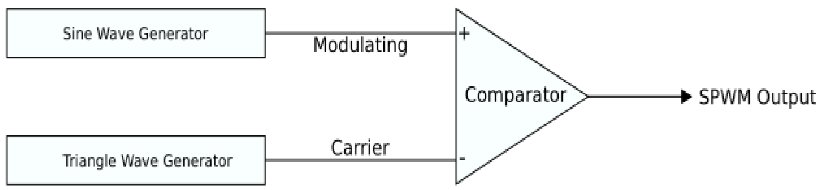

Figure 2.19. A schematic of sinusoidal PWM modulation

2.3.5.1. Direct Digital Synthesis Method

A direct digital synthesizer (DDS) produces a frequency-adjustable analog waveform by using a digital signal source. It is a digital method to generate high frequency waveforms. Generally, the waveform is a sinusoidal wave. To generate the waveform, a look-up table is used. This table outputs the amplitude of the waveform at that instant. After going through the whole lookup table, a time series of amplitudes resembling the waveform is generated. Lastly, the digital time series is applied to a digital-to-analog converter (DAC) to obtain the desired waveform. The frequency of the waveform can be adjusted by either changing the reference clock frequency or tuning word. Depending on these values, the number of the output of the lookup table block will be changed thus the frequency of the wave changes too (Murphy & Slattery, 2004). The entire process is summarized in a block diagram given in Figure 2.20.

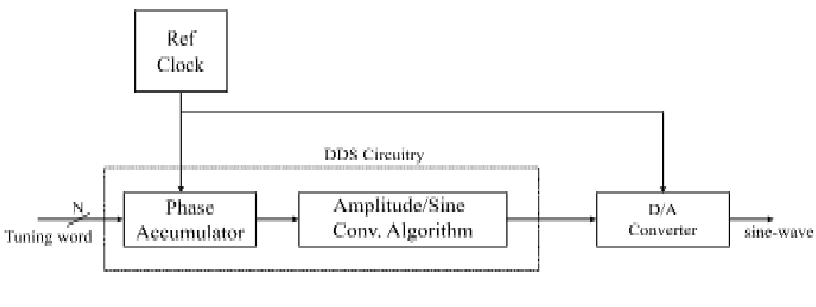

Figure 2.20. Direct digital synthesis method

3. OVERVIEW OF SENSORLESS BLDCM

A sensorless BLDCM drive system consists of a controller, inverter circuit, feedback system, and a BLDCM. In this section, the design of BLDCM and the main components of drive system are discussed. A generic sensorless BLDCM drive system is given in Figure 3.1.

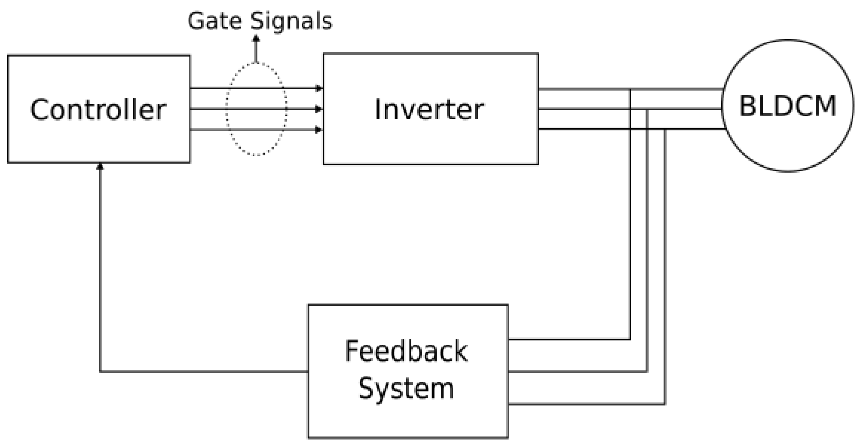

Figure 3.1. Sensorless BLDCM drive

3.1. Design of BLDCM

BLDCMs are used in many different application areas. Thereby design process of BLDCM is highly involved with the application requirements. The stator and rotor are the two main parts of a BLDCM. Permanent magnets are placed on the rotor, and windings are on the stator. More information about the design process of the rotor and stator is given in the below sections.

3.1.1. Stator Structure of BLDCM

BLDCM's stator is made with laminated steel, and the windings are inserted into the slots. Each winding is made up of interconnected coils, which are distributed across the stator to obtain the desired number of poles (Yedamale, 2003). The concentrated windings are commonly used to generate a trapezoidal back-EMF waveform, while the distributed windings are used to obtain a sinusoidal back-EMF shape. The visuals of concentrated and distributed windings are shown in Figure 3.2 and Figure 3.3, respectively.

Figure 3.2. Concentrated stator windings.

Figure 3.3. Distributed stator windings.

3.1.2. Rotor Structure of BLDCM

The rotor of BLDCM can be inside or outside of the stator. The rotor inside the stator is known as inrunner BLDCM, while the rotor located around the stator is called outrunner BLDCM as given in Figure 3.4 and Figure 3.5. The permanent magnets are placed on the rotor of BLDCM. The shape of magnets affects cogging torque and back-EMF waveform (Ruangsinchaiwanich, Zhu, & Howe, 2005). In addition, the magnets can be placed inside or outside of the rotor, which called as interior permanent magnet and surface permanent magnet, respectively.

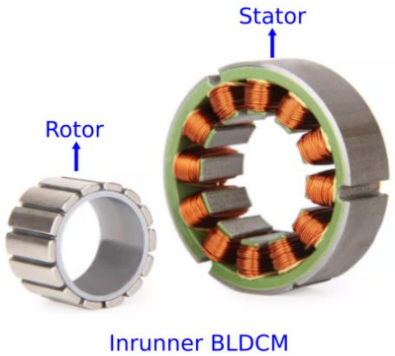

Figure 3.4. Inrunner BLDC motor ("T-Motor CubeMars RI50 Çerçevesiz Inrunner Motor 12V-48V Motor BLDC Motor Düşük Dişli Tork," n.d.)

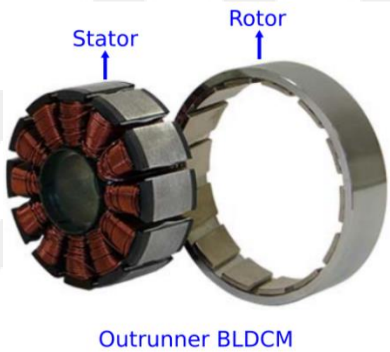

Figure 3.5. Outrunner BLDC motor ("Small High Torque Motor," n.d.)

3.2. Modeling of BLDCM

The electrical model of a BLDCM given in Figure 3.6 is constructed by considering the resistive and inductive characteristics of each phase and inductive couplings between them known as mutual effect. Losses such as iron and stray are ignored in the model (Kılıçkır, 2019; Li, Zheng, & Ren, 2017).

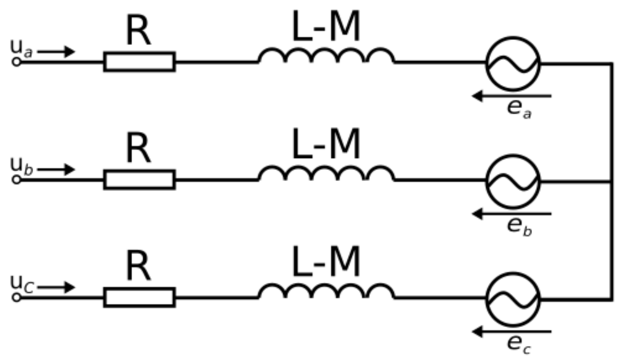

Figure 3.6. The electrical model of a BLDCM

Before the mathematical derivation of the BLDCM voltage equation, the below assumptions are made where *R*, *L*, and *M* represent stator resistance, current, and inductance, respectively for each phase;

$$R_a = R_b = R_c = R \tag{3.1}$$

$$L_a = L_b = L_c = L \tag{3.2}$$

$$L_{ab} = L_{bc} = L_{ca} = M \tag{3.3}$$

The voltage equation in matrix for is;

$$\begin{pmatrix} u_a \\ u_b \\ u_c \end{pmatrix} = \begin{pmatrix} R & 0 & 0 \\ 0 & R & 0 \\ 0 & 0 & R \end{pmatrix} \begin{pmatrix} i_a \\ i_b \\ i_c \end{pmatrix} + \begin{pmatrix} L-M & 0 & 0 \\ 0 & L-M & 0 \\ 0 & 0 & L-M \end{pmatrix} \frac{d}{dt} \begin{pmatrix} i_a \\ i_b \\ i_c \end{pmatrix} + \begin{pmatrix} e_a \\ e_b \\ e_c \end{pmatrix} \tag{3.4}$$

Back-EMF voltages are dependent upon rotor speed, rotor position, and the motor constant. Equations for each phase back-EMF are given below where e_a, e_b, and e_c are induced back-EMF on each phase, ω is rotational speed, K_e is the back-EMF constant, and $f(\theta)$ is the normalized function of the rotor position (Tsai, Quy, Wu, & Tseng, 2011).

$$e_a = wK_e f(\theta) \tag{3.5}$$

$$e_b = wK_e f(\theta - \frac{2\pi}{3}) \tag{3.6}$$

$$e_c = wK_e f(\theta + \frac{2\pi}{3}) \tag{3.7}$$

$$f(x) = \begin{cases} 0 < \theta \le \frac{\pi}{3} & 1 \\ \frac{\pi}{3} < \theta \le \frac{2\pi}{3} & \frac{(\frac{\pi}{2} \text{-} \theta)6}{\pi} \\ \frac{2\pi}{3} < \theta \le \frac{4\pi}{3} & -1 \\ \frac{4\pi}{3} < \theta \le \frac{5\pi}{3} & \frac{(\theta - \frac{3\pi}{2})6}{\pi} \\ \frac{5\pi}{3} < \theta \le 2\pi & 1 \end{cases} \tag{3.8}$$

The instantaneous power generated by BLDCM is the sum of multiplied each phase back-EMF and currents.

$$P = e_a i_a + e_b i_b + e_c i_c \tag{3.9}$$

Electromagnetic torque equations of BLDCM are given below where T_e is electromagnetic torque.

$$P = T.w \tag{3.10}$$

$$T_e = \frac{P}{w} = \frac{e_a i_a + e_b i_b + e_c i_c}{w} \tag{3.11}$$

3.3. Working Principles of BLDCM

The principle of operation is to generate the force on the rotor with the interaction of stator and rotor magnetic fields. Stator coils are excited to form the stator magnetic field, which causes movement on the rotor and the direction of the rotor magnetic field changes. Therefore the stator magnetic field has to be changed because the maximum torque occurs when the angle between these fields is 90° (Yedamale, 2003). This is achieved by changing the orientation of the current in BLDCM, which alters the direction of the magnetic field, and the continuous operation of BLDCM is ensured. This process is called commutation that is depicted in Figure 3.7 for 120° commutation. The commutation points can be found by various rotor position detection techniques explained in the literature review.

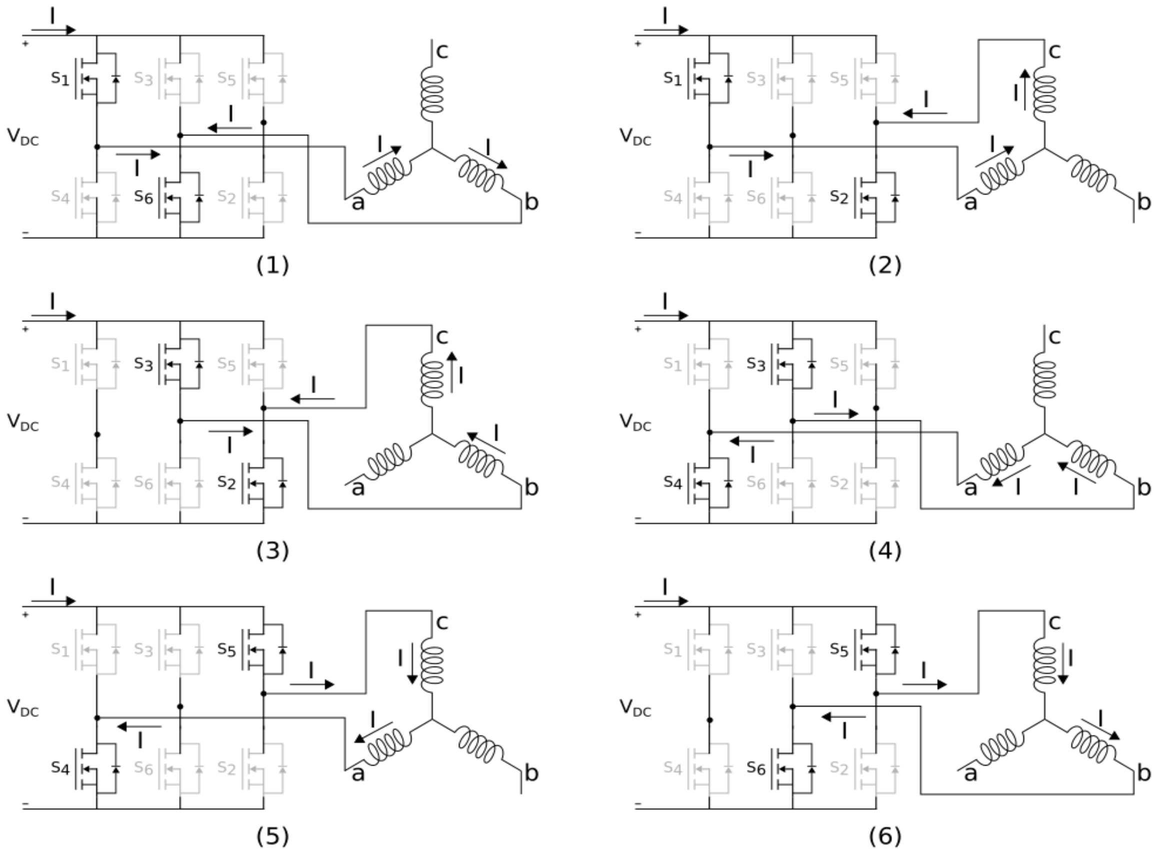

Figure 3.7. 120° commutation illustrated for each of six-step

The back-EMF detection-based techniques are commonly used to detect the rotor position in the sensorless control of BLDCM. Induced back-EMF waveform for a three-phase and two poles BLDCM is given in Figure 3.8. As it was expressed, the sloping parts of back-EMF are used to determine the rotor position and it is known that 30° delay given after the zero crossing of a sloping part is the indicator for a new commutation state. This property is used by 120°

commutation method for sensorless control. Because the method does not energize the motor phases on the sloping parts, therefore zero-crossings of the back-EMF can be measured.

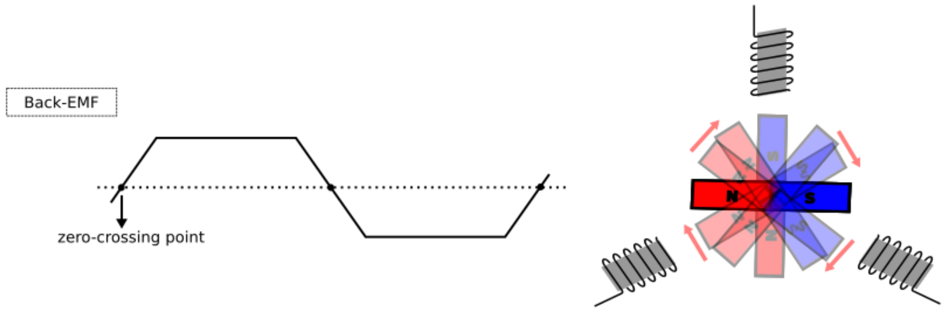

Figure 3.8. Induced back-EMF waveform on a phase for a full rotation

4. MATERIALS AND METHODS

4.1. Power Circuit Design of BLDCM

The power circuit of BLDCM is responsible for the continuous operation of BLDCM. The circuit achieves this objective by energizing the motor windings at the correct instants. By energizing the motor windings, a rotating magnetic field in the stator is created that follows the rotor magnetic field. This rotation of the stator field is performed by an inverter circuit that switches the power on and off in the power circuit, wherein the switching instants of the inverters are decided by a controller. The controller operates on the back-EMF feedback signals, which are obtained by a resistor divider subcircuit and provides switching signals to the inverter. The power circuit components will be explained in the below subsections.

4.1.1. Microcontroller

The microcontroller is responsible for processing the back-EMF signal and generating commutation signals for the inverter. In this thesis, Arduino Nano board has been chosen for generating commutation signals and processing back-EMF signals due to its small size, low-cost, reliability, etc. Its pinout and technical properties are given in Fig 4.1 and Table 4.1, respectively.

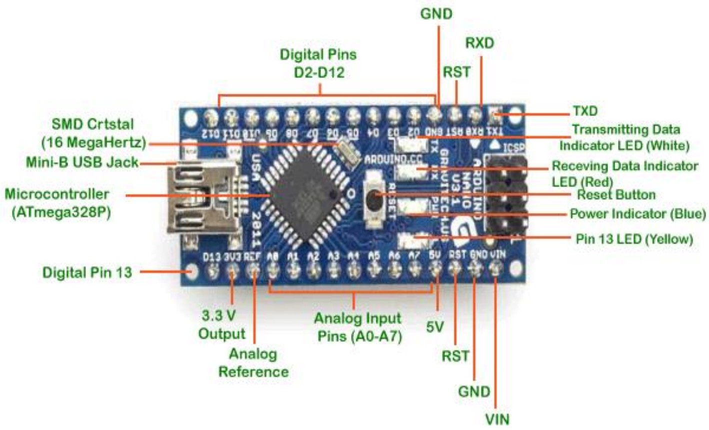

Figure 4.1. Arduino NANO and pin descriptions ("Arduino Nano Pinout," n.d.)

Table 4.1. Arduino Nano technical details (Watson, 2018).

Microcontroller	Atmega328p
Cryristal Oscillator	16MHz
Input Voltage	6V-12V
Maximum Current Rating	40mA
D0-D13	Digital Input / Output pins
A0-A7	Analog Input / Output pins
Pin # 3, 5, 6, 9, 10, 11	Pulse Width Modulation (PWM) pins
D2 & D3	External Interrupt pins

4.1.2. Inverter Circuit

In the drive system, inverter circuit is directly connected to the motor phases. It commutates BLDCM by changing the on-off states of its switching elements. The switching elements could be transistors, MOSFETs, and IGBTSs. The switching element is chosen by taking into account of switching frequency of the application requirements and losses (ATAN, 2007). In this thesis, two L298N motor drive module is used to commutate BLDCM and transistors are used as switching elements in the module. The L298 is an integrated monolithic circuit and it is a high voltage, high current dual full-bridge driver designed to accept standard TTL logic levels and drive inductive loads such as relays, solenoids, DC and stepping motors ("DUAL FULL-BRIDGE DRIVER," n.d.). The figure of the motor drive module with pin descriptions and technical details are given in Figure 4.2 and Table 4.2, respectively.

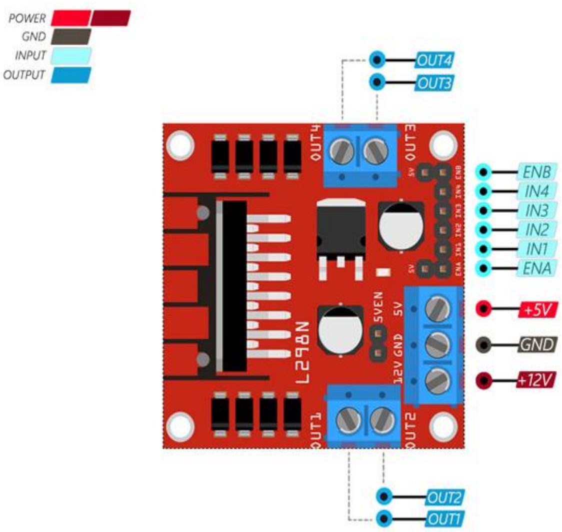

Figure 4.2. L298N motor drive module

Table 4.2. L298N motor driver ("L298n Dual Full-Bridge Motor Driver," n.d.).

Motor Driver	L298N
Motor Channels	2
Maximum operation voltage	46V
Peak output current per channel	2A
Minimum logic voltage	4.5V
Maximum logic voltage	7V

For this thesis, a low-cost inverter circuit is developed for the experimental studies. Printed circuit board (PCB) design of the power circuit and hardware implementation are illustrated in Figure 4.3 a) and Figure 4.3 b). At the PCB circuit, red and yellow lines represent traces and jumpers, respectively.

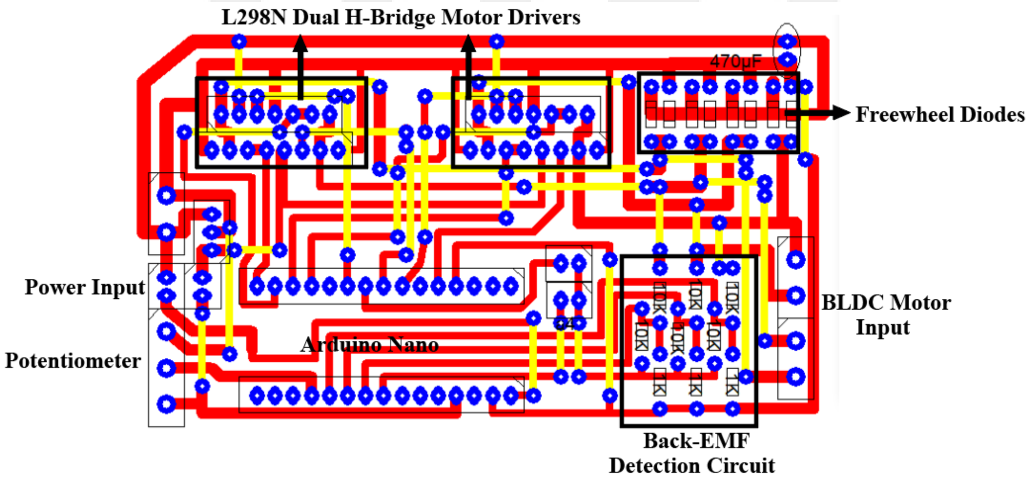

a)

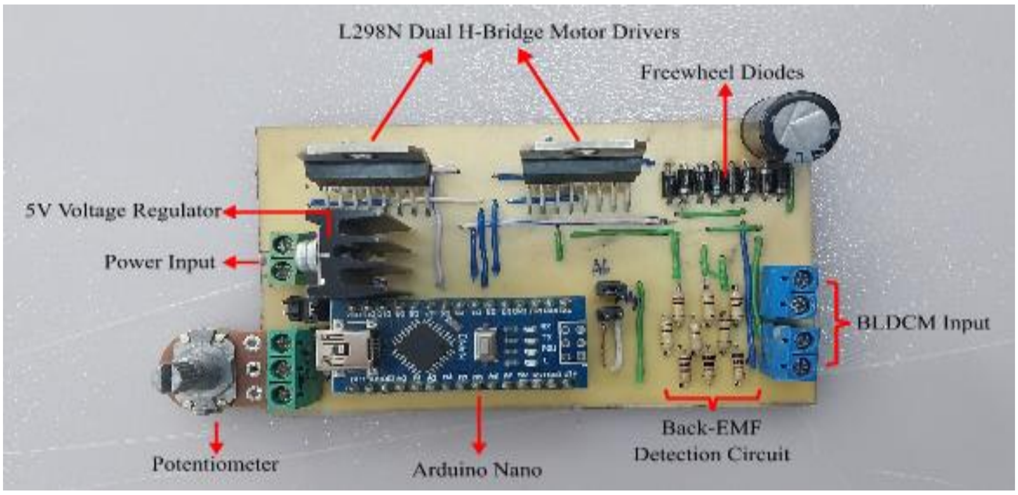

b)

Figure 4.3. a) PCB design of power circuit b) Sensorless BLDCM drive circuit

4.1.3. Back-EMF Feedback Circuit

The 120° commutation method energizes two out of three-phase windings and leaves one phase floating. The floating phase is used to detect back-EMF and the time required to change the commutation state is calculated.

In star-connected BLDCMs, usually neutral point connection is not available; therefore, a virtual neutral point is created to measure back-EMF. In theory, the point is expected to be at the same potential as the center of a star-connected motor. By this method zero-crossings of unenergized phase back-EMF can be detected easily (Shao, Nolan, Teissier, & Swanson, 2002).

4.1.4. BLDC Motor

A sensorless BLDCM used specifically for multi-rotor aircraft application is preferred for the experimental study. The figure of the BLDCM and technical specifications of the motor is given in Figure 4.4 and Table 4.3, respectively.

Figure 4.4. iPower iBM2217Q 880KV sensorless BLDCM

Table 4.3. Technical information of sensorless BLDCM used in the experimental study (“IPower IBM2217Q 880KV,” n.d.).

KV	880
Internal Resistance	107 mΩ
Phase Inductance	0.005mH
No-load current	0.8A
Continuous Current	14.8A
Max Watts	210W
Lipo Cells	2-4s
Weight	94g
Dimensions	28x36mm
Wire Length	450mm
Shaft Diameter	4.0mm

In order to apply various commutation methods Proteus simulation software described in Figure 4.5 and real-time experimental environment given in Figure 4.6 are used. For the experimental studies, a 10x4.5 inch (1045r) is used as propeller on the drone motor. The speed of BLDCM is adjusted by a potentiometer connected to the Arduino. As potentiometer reading changes, Arduino updates the frequency of the switching signals accordingly. Thus, the speed of the motor is modified.

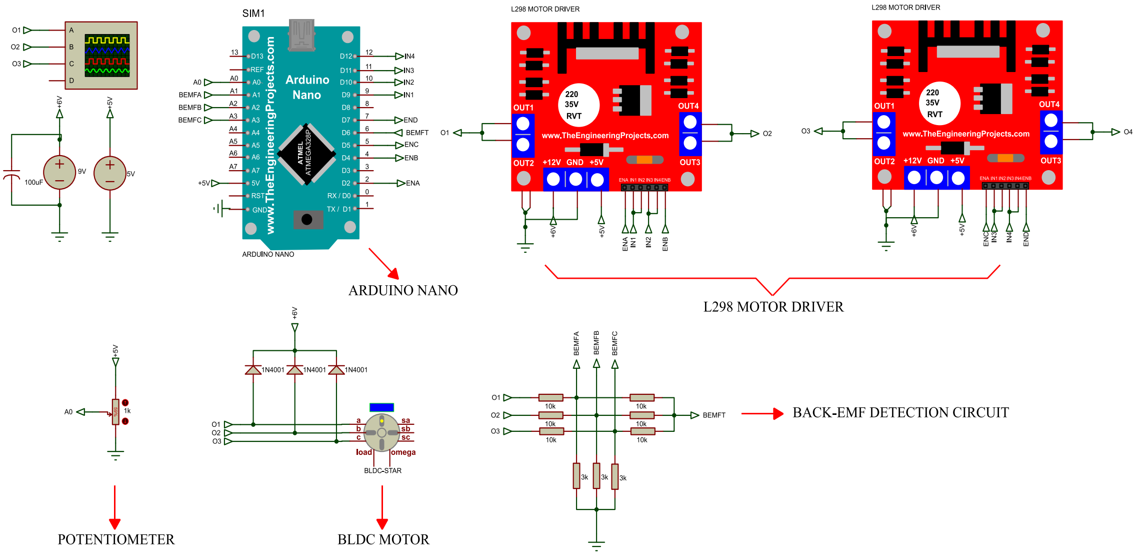

Figure 4.5. Simulation circuit

Figure 4.6. The experimental setup

4.2. Case Studies

The performance of the commutation methods is evaluated as follows. Firstly, the performance tests of 120°, 150°, and 180° commutation, and the DDS method is realized as open-loop. Secondly, back-EMF-based closed-loop 120° commutation is realized in two case studies by which one of them uses a comparator and the other analog to digital conversion (ADC) unit to analyze the back-EMF. Thirdly, the performance of the proposed three-step method is tested. Lastly, the proposed method is compared with a good-performing back-EMF-based 120°

commutation method. In addition, the overall comparison of applied methods is conducted in one case study.

It is important to note that, the voltage spikes seen on the waveforms when changing to a new commutation state can be stem from variety sources such as limited calculation frequency of microcontroller and analog to digital conversion (ADC) error in signal processing. An important consequence of these spikes is that it generates torque ripples which is a serious problem where precise motion control is required (Lee, 2019). Therefore, many studies are conducted to reduce the torque ripples by proposing different compensation methods (A. C. Lee, Wang, & Fan, 2016; Wang et al., 2021).

4.2.1. Case Study 1: 120° Commutation Results

120° commutation steps described in Figure 2.12 a) were applied to the BLDCM via the drive circuit without position feedback. Minimum and maximum attainable speed test results for the method are given in Table 4.4. It is observed that thrust was measured as 0 gram-force (gf) and the current drawn was 2.45A at the minimum speed of 186rpm. At the maximum speed of 1526rpm, thrust was measured as 33gf and the current drawn was 2.60A. According to the test results, it can be said that the increasing of current value calculated as 6.1%. The maximum attainable speed is reached when the drive signal is at the frequency of 193Hz.

Table 4.4. Performance results of 120° commutation method.

	Minimum Speed Results	**Maximum Speed Results**
Voltage (V)	12	12
Current (A)	2.45	2.60
Speed (rpm)	186	1526
Thrust (gf)	0	33

The simulation and experimental waveforms of line-to-line and phase-to-ground voltages are given in Figure 4.7. The simulation and experimental waveforms are consistent with to each other.

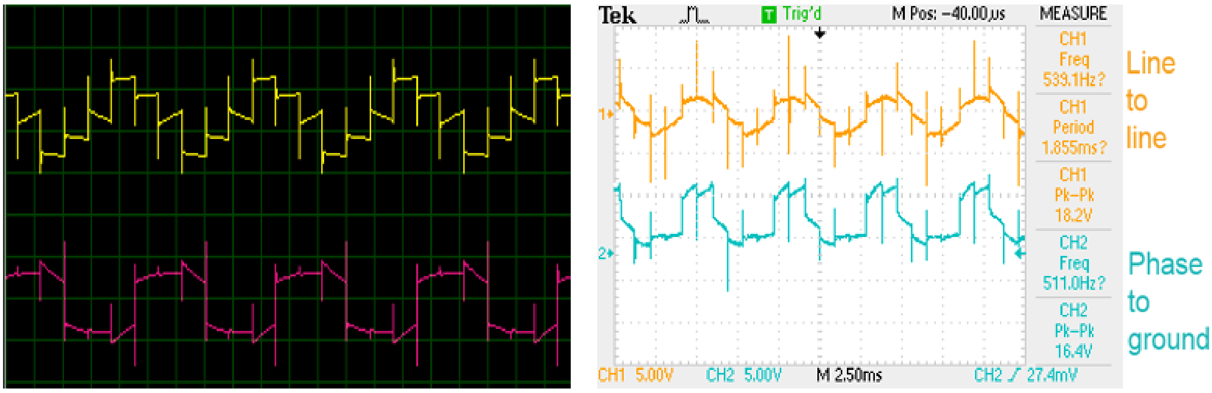

Figure 4.7. Simulation and oscilloscope waveforms are shown respectively.

4.2.2. Case Study 2: 150° Commutation Results

150° commutation steps described in Figure 2.14 a) were applied to the BLDCM via the drive circuit without position feedback. Minimum and maximum attainable speed test results for the method are given in Table 4.5. It is observed that thrust was measured as 0gf and the current drawn was 2.73A at the minimum speed of 178rpm. At the maximum speed of 1327rpm, thrust was measured as 25gf and the current drawn was 2.90A. According to the test results, it can be said that the increasing of current value was calculated as 6.2%. The maximum attainable speed is reached when the drive signal is at the frequency of 153Hz.

Table 4.5. Performance results of 150° commutation method.

	Minimum Speed Results	**Maximum Speed Results**
Voltage (V)	12	12
Current (A)	2.73	2.90
Speed (rpm)	178	1327
Thrust (gf)	0	25

The simulation and experimental waveforms of line-to-line and phase-to-ground voltages are given in Figure 4.8. The simulation and experimental waveforms are consistent with to each other.

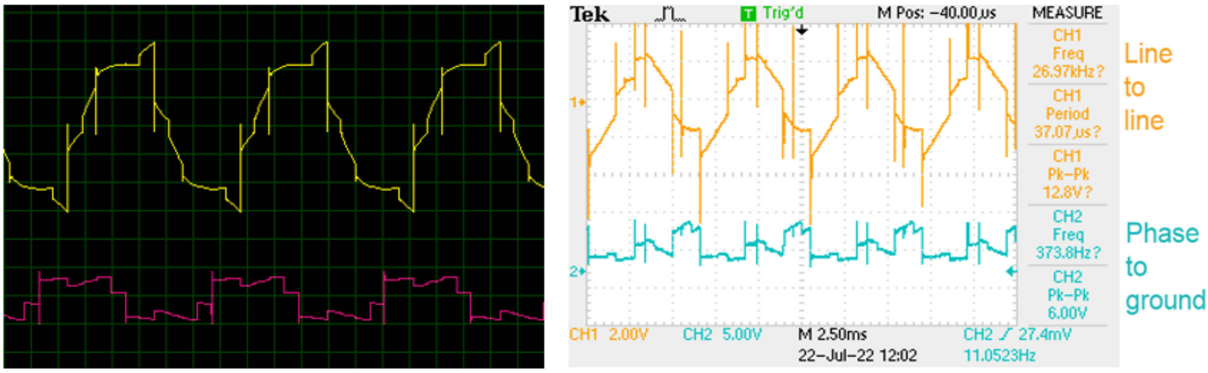

Figure 4.8. Simulation and oscilloscope waveforms are shown respectively.

4.2.3. Case Study 3: 180° Commutation Results

180° commutation steps described in Figure 2.16 a) were applied to the BLDCM via the drive circuit without position feedback. Minimum and maximum attainable speed test results for the method are given in Table 4.6. It is observed that thrust was measured as 0gf and the current drawn was 3.01A at the minimum speed of 178rpm. At the maximum speed of 1480rpm, thrust was measured as 30gf and the current drawn was 3.08A. According to the test results, it can be said that the increasing of current value was calculated as 2.32%. The maximum attainable speed is reached when the drive signal is at the frequency of 167Hz.

Table 4.6. Performance results of 180° commutation method.

	Minimum Speed Results	**Maximum Speed Results**
Voltage (V)	12	12
Current (A)	3.01	3.08
Speed (rpm)	178	1480
Thrust (gf)	0	30

The simulation and experimental waveforms of line-to-line and phase-to-ground voltages are given in Figure 4.9. The simulation and experimental waveforms are consistent with to each other.

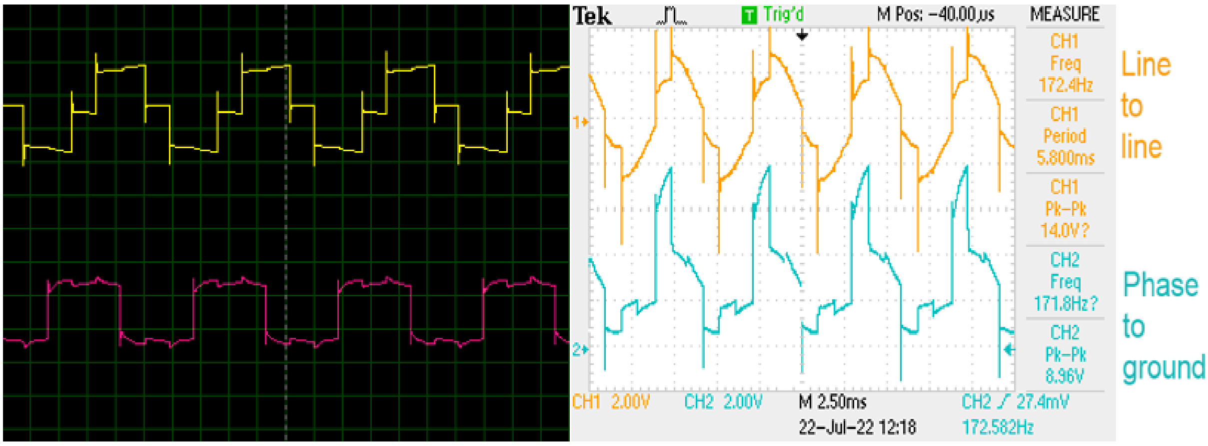

Figure 4.9. Simulation and oscilloscope waveforms are shown respectively.

4.2.4. Case Study 4: DDS Method

The DDS-based sine wave generation method is used in open-loop control of BLDCM in this case study ("PWM Sine Wave Generation," n.d.). The methodology used for the case study is described as follows. Sinusoidal waveform amplitudes are represented in the range of 0 to 255 and stored in the look-up table. The reference clock frequency is selected as 1024Hz and the timer1 interrupt of microcontroller is set to 30.88kHz to obtain the waveform given in Figure 4.10. Also the frequency of the waveform is changed with the potentiometer by readjusting the tuning word. Minimum and maximum attainable speed performance results for the DDS method are given in Table 4.7. According to these results, it can be said that the decrease in current value was calculated as 16.8%.

Table 4.7. Performance results of the DDS method.

	Minimum Speed Results	**Maximum Speed Results**
Voltage (V)	12	12
Current (A)	2.38	1.98
Speed (rpm)	143.8	2116
Thrust (gf)	0	70

Voltage magnitudes of line-to-line and phase-to-ground waveforms are acquired. The simulation and experimental waveform look similar to each other. The maximum attainable speed is reached when the drive signal is at the frequency of 238Hz.

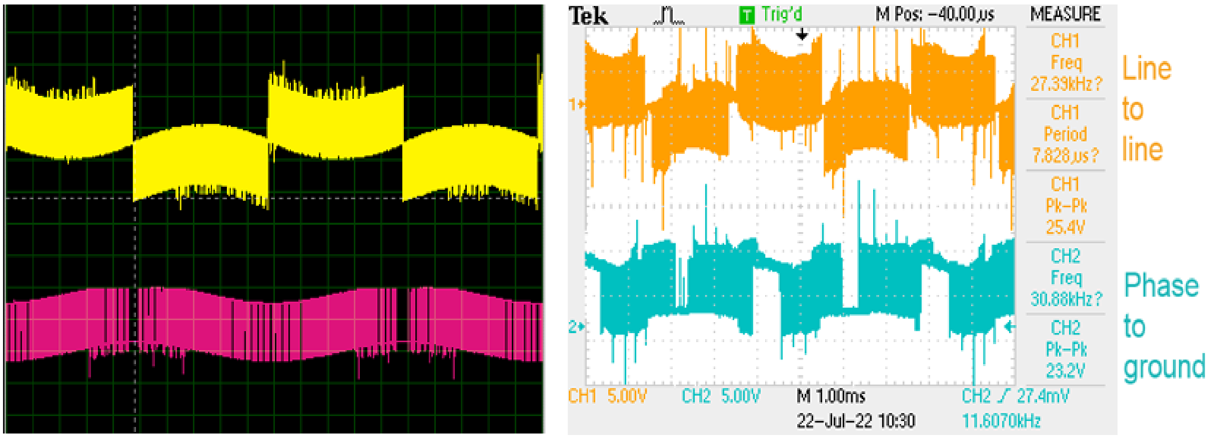

Figure 4.10. Simulation and oscilloscope waveforms are shown respectively.

4.2.5. Case Study 5: Analog to Digital Conversion-Based Commutation

Switching signals for inverters are generated based on ADC of back-EMFs and arithmetic manipulation in software. The sampling frequency of the ADC unit is adjusted to 2MHz. After the detection of zero crossing of phase back-EMF, the commutation sequence is followed and the next commutation state is utilized. Applied drive signal frequency to the BLDCM changes according to the reference speed signal that is adjusted by the potentiometer connected to the microcontroller. The commutation sequence for 120° commutation method is described in section 2.3.1. Minimum and maximum attainable speed performance results for the ADC method are given in Table 4.8.

Table 4.8. Performance results of ADC-based back-EMF method.

	Minimum Speed Results	**Maximum Speed Results**
Voltage (V)	12	12
Current (A)	2.32	2.17
Speed (rpm)	1483	2361
Thrust (gf)	33	85

Voltage magnitudes of line-to-line and phase-to-ground waveforms are acquired. The simulation and experimental waveform look similar to each other. The maximum attainable speed is reached when the drive signal is at the frequency of 250Hz. The simulation and experimental waveform are given in Figure 4.11.

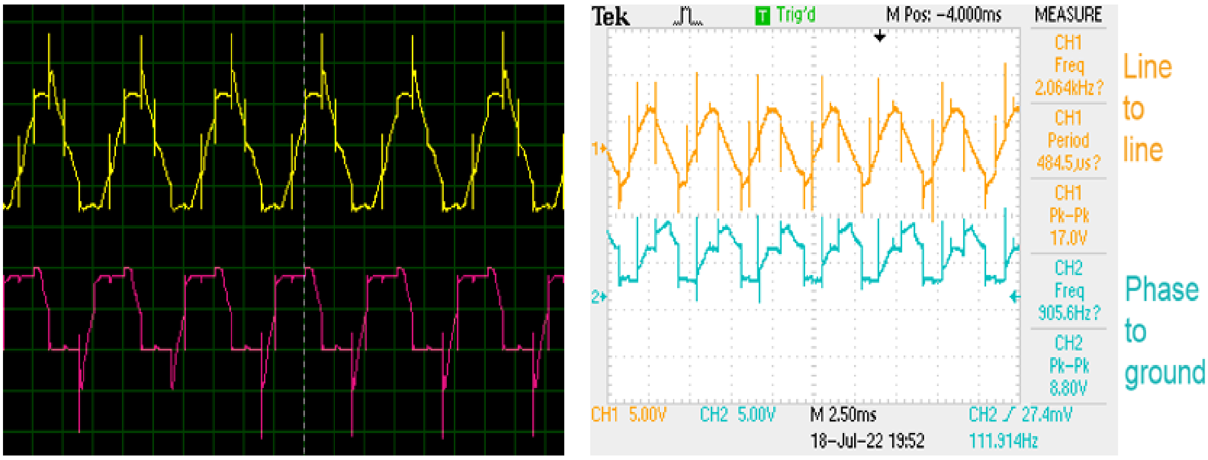

Figure 4.11. Simulation and oscilloscope waveforms are shown respectively.

4.2.6. Case Study 6: Comparator Utilized Based Commutation Method

In this method, the internal comparator unit of Atmega328p is used to detect the zero crossing points of back-EMFs. After detecting a zero crossing point interrupt routine takes over the execution of the program and the next commutation state is applied to the BLDCM. Minimum and maximum attainable speed performance results for the method is given in Table 4.9.

Table 4.9. Performance results of interrupt-based back-EMF method.

	Minimum Speed Results	**Maximum Speed Results**
Voltage (V)	12	12
Current (A)	0.72	2.24
Speed (rpm)	130	2243
Thrust (gf)	0	76

Voltage magnitudes of line-to-line and phase-to-ground waveforms are acquired. The simulation and experimental waveform look similar to each other. The maximum attainable speed is reached when the drive signal is at the frequency of 256Hz. The simulation and experimental waveform are given in Figure 4.12.

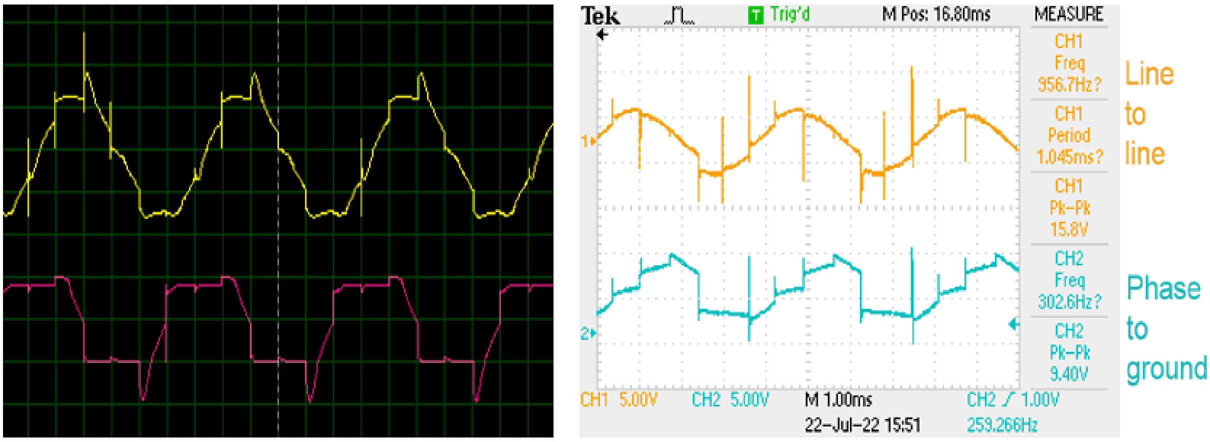

Figure 4.12. Simulation and oscilloscope waveforms are shown respectively.

4.2.7. Case Study 7: The Proposed Three-Step Method

The proposed method energizes two phases and leaves one phase floating as in 120° commutation. Three out of six-step are applied with back-EMF measurements by using the ADC unit. The method executes one commutation step and skips the other. For example, 1, 3, 5, or 2, 4, and 6 steps are used to run BLDCM in Figure 3.7. Intermediate steps are skipped. The sampling frequency of the ADC unit is adjusted to 1MHz to increase the sensitivity of the measurements due to low back-EMF voltage. The performance evaluation is realized and the results are given in Table 4.10.

Table 4.10. Performance results of the proposed three-step commutation method.

	Minimum Speed Results	**Maximum Speed Results**
Voltage (V)	12	12
Current (A)	2.38	2.30
Speed (rpm)	1387	1865
Thrust (gf)	27	53

Voltage magnitudes of line-to-line and phase-to-ground waveforms are are acquired. The simulation and experimental waveform look similar to each other. The maximum attainable speed is reached when the drive signal is at the frequency of 200Hz. The simulation and experimental waveform are given in Figure 4.13.

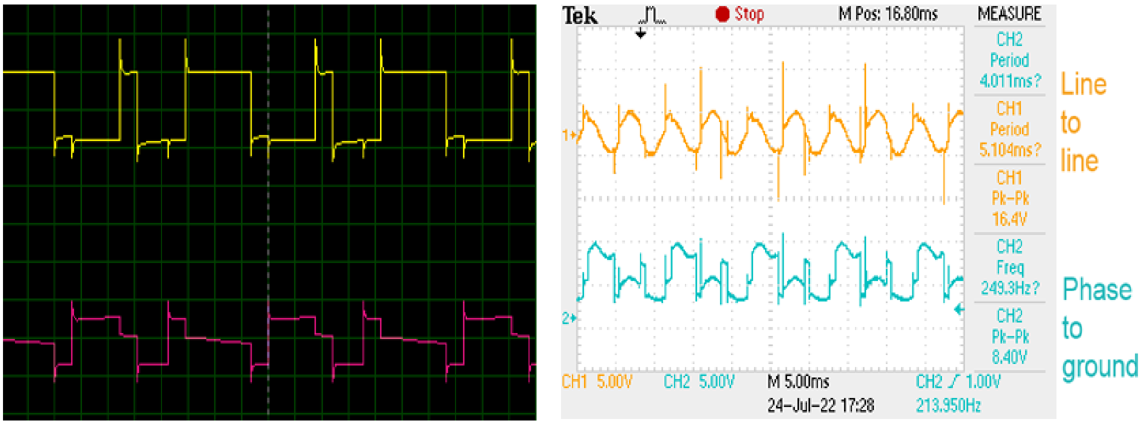

Figure 4.13. Simulation and oscilloscope waveforms are shown respectively.

5. RESULTS AND DISCUSSIONS

In the results and discussions section, two case studies are examined. The first case study evaluates implemented open-loop control methods and back-EMF-based closed-loop control methods. In the second case study, the proposed method is compared with the best-performing control method in the first case study.

5.1. Case Study 8: Performance Comparison of Applied Methods

In this case study, commonly used open-loop control methods and closed-loop back-EMF-based methods are compared. Comparison is based on thrust, maximum rpm, and current drawn measurements of BLDCM. Table 5.1 is filled with acquired experimental data at maximum speed and used as basis to compare implemented control methods.

Table 5.1. Performance comparison table of experimental studies.

	Voltage (V)	**Current (A)**	**Maximum rpm (rev/min)**	**Thrust(gf)**
120° commutation	12	2.60	1526	33
150° commutation	12	2.90	1327	25
180° commutation	12	3.08	1480	30
DDS-based SPWM	12	1.98	2116	70
Interrupt-based method	12	2.24	2243	76
ADC unit-based method	12	2.17	2361	85

According to the results, the DDS method has lower power consumption due to that the current drawn is less than other applied control methods and higher thrust, maximum speed, and wider speed range than 120°, 150°, and 180° commutation. However, the back-EMF-based methods achieved higher maximum speed and thrust than the DDS method. Furthermore, it is observed that 180° commutation has drawn more current than other methods since it energizes three stator windings at all times.

It can be seen that the closed-loop methods outperform open-loop methods in thrust and speed at maximum speed. In addition, these methods have lower current drawings than open-loop methods except DDS method. It is clear from the table that the back-EMF-based 120° commutation in which the ADC unit is used has higher speed and thrust than other methods. Thereby it is selected as the reference to evaluate the performance of the proposed method in the second case study.

5.2. Case Study 9: Performance Comparison of the Proposed Method

In this case study, performance of the proposed method is compared with the back-EMF-based 120° commutation in which the ADC unit is used. The maximum speed and thrust for the proposed method are found 1865rpm and 53gf, respectively by adjusting the level of the potentiometer. At the same level of the potentiometer (same speed reference signal), speed and thrust for the back-EMF-based 120° commutation are found 1592rpm and 39gf, respectively. Therefore, it can be concluded from Table 5.2 that the proposed method has better results than the compared method. The maximum attainable speed of the proposed method can be improved in future works.

Table 5.2. Experimental results of back-EMF-based ADC unit utilized 120° commutation and the proposed method.

	Voltage(V)	**Current(A)**	**Rpm(rev/min)**	**Thrust(gf)**
ADC unit based method	12	2.60	1592	39
Three-step method	12	2.30	1865	53

6. CONCLUSIONS

BLDCMs have been widely used in various fields like household appliances, drones, automobile industry, robotics, and aerospace applications due to their high efficiency, compact size, high dynamic response, controllability, and reliability. In the control algorithm of BLDCMs, sensorless control has gained more attention from researchers and many techniques have been developed to detect the rotor position with various approaches such as direct detection of back-EMF, estimation of back-EMF by using observer theory, artificial intelligence, flux-linkage, inductance variation. Generally, these techniques are coupled with a controller(s) and a commutation method mainly, 120°, 150°, and 180° commutation, SVPWM, and SPWM.

In this thesis, a sensorless BLDCM is controlled by using several open-loop and closed-loop methods. The case studies are realized experimentally and in simulations. Proteus software is used for simulation studies. For experimental studies, a prototype inverter circuit is designed, and an Arduino Nano board, which includes the ATmega328P microcontroller, is used. In the case studies, maximum and minimum speed tests of the methods are realized. Thrust and current drawn at these speeds are tabulated in the respective tables. In addition, the result tables are used in the performance comparison of the methods. In addition, graphs of voltage signals applied to BLDCM in experiments and simulations are compared. Furthermore, a back-EMF-based three-step commutation is proposed. The proposed method is derived from the 120° commutation by which even or odd consecutive steps of the 120° commutation are used. In order to validate the proposed method, the aforementioned test procedure is applied.

According to the results, the DDS method has lower power consumption due to that the current drawn is less than other applied control methods and higher thrust, maximum speed, and wider speed range than 120°, 150°, and 180° commutation. However, the closed-loop methods outperform open-loop methods at maximum speed and thrust. In addition, these methods have lower current drawings than open-loop methods except the DDS method. In this last case study, the proposed method is compared with the back-EMF-based 120° commutation in which the

ADC unit is used. The results have shown that, better results are produced with the proposed method than the compared method.

REFERENCES

Al-Adsani, A. S., Alsharidah, M. E., & Beik, O. (2021). BLDC Motor Drives: A Single Hall Sensor Method and a 160° Commutation Strategy. *IEEE Transactions on Energy Conversion*, *36*(3), 2025–2035. https://doi.org/10.1109/TEC.2020.3046183

Arduino Nano Pinout. (n.d.). Retrieved December 1, 2022, from https://www.javatpoint.com/arduino-nano-pinout

ATAN, Ö. (2007). Fırçasız da motorunun modellenmesi ve pwm yöntemiyle kontrolü.

Attar, A., Bouchnaif, J., & Grari, K. (2021). Control of Brushless DC motors using sensorless Back-EMF integration method. Materials Today: Proceedings, 45, 7438–7443. https://doi.org/10.1016/j.matpr.2021.01.861

Bayır, F. (2019). Design of a Sensorless Bldc Motor Driver Using Field Oriented Driver Using Field Oriented.

Becerra, RC., Jahns, TM., Ehsani, M. (1991). Four-quadrant sensorless brushless ECM drive. In Conference Procedings - IEEE Applied Power Electronics Conference and Exhibition, 202–209. https://doi.org/10.1109/apec.1991.146165

Champa, P., Somsiri, P., Wipasuramonton, P., & Nakmahachalasint, P. (2009). Initial rotor position estimation for sensorless brushless DC drives. *IEEE Transactions on Industry Applications*, *45*(4), 1318–1324. https://doi.org/10.1109/TIA.2009.2023355

Cheng, K. Y., & Tzou, Y. Y. (2003). Design of a Sensorless Commutation IC for BLDC Motors. IEEE Transactions on Power Electronics, 18(6), 1365–1375. https://doi.org/10.1109/TPEL.2003.818867

Consoli, A., Musumeci, S., Testa, A., & Raciti, A. (1994). Sensorless Vector and Speed Control of Brushless Motor Drives. IEEE Transactions on Industrial Electronics, 41(1), 91–96. https://doi.org/10.1109/41.281613

Ding, X., & Liu, Z. (2022). Position Sensorless Control and Real-time Commutation Delay Compensation of a Micro BLDC Motor. 1–5. https://doi.org/10.1109/itecasia-pacific56316.2022.9942004

DUAL FULL-BRIDGE DRIVER. (n.d.). Retrieved December 27, 2022, from https://www.sparkfun.com/datasheets/Robotics/L298_H_Bridge.pdf

Fonseca, P., Nielsen, S. B., & Both, D. (2011). VSDs for Electric Motor Systems. 1–109. Retrieved from http://www.watergymex.org/Watergy Toolkit/resources/54_VSDs_Save_Energy.pdf

Gamazo-Real, J. C., Vázquez-Sánchez, E., & Gómez-Gil, J. (2010). Position and speed control of brushless dc motors using sensorless techniques and application trends. Sensors, 10(7), 6901–6947. https://doi.org/10.3390/s100706901

Gujjar, M. N., & Kumar, P. (2017). Comparative analysis of field oriented control of BLDC motor using SPWM and SVPWM techniques. RTEICT 2017 - 2nd IEEE International

Conference on Recent Trends in Electronics, Information and Communication Technology, Proceedings, 2018-Janua, 924–929. https://doi.org/10.1109/RTEICT.2017.8256733

Iizuka, K., Uzuhashi, H., Kano, M., Endo, T., & Mohri, K. (1985). Microcomputer Control for Sensorless Brushless Motor. IEEE Transactions on Industry Applications, IA-21(3), 595–601. https://doi.org/10.1109/TIA.1985.349715

iPower iBM2217Q 880KV. (n.d.). Retrieved July 21, 2022, from http://osiworx.com/product/ipower-ibm2217q-880kv/

Jang, G. H., Park, J. H., & Chang, J. H. (2002). Position detection and start-up algorithm of a rotor in a sensorless BLDC motor utilising inductance variation. IEE Proceedings: Electric Power Applications, 149(2), 137–142. https://doi.org/10.1049/ip-epa:20020022

Jani, Y. (n.d.). Implementing Embedded Speed Control for Brushless DC Motors Part 2 : Introduction 180-degree modulation. 27.

Khambhadiya, H., & Dhaneria, A. (2021). Sensorless Control Method of 3-Phase BLDC Motor Through Back-EMF Observer. International Conference on Advances in Electrical, Computing, Communication and Sustainable Technologies (ICAECT), 1–5. IEEE.

Kim, T., Lee, H.W., Ehsani, M., & Ehsani, M. (2007). Position sensorless brushless DC motor generator drives: review and future trends. IET Electric Power Applications. https://doi.org/10.1049/iet-epa

Kim, J. S., & Sul, S. K. (1995). High performance PMSM drives without rotational position sensors using reduced order observer. Conference Record - IAS Annual Meeting (IEEE Industry Applications Society), 1, 75–82. https://doi.org/10.1109/ias.1995.530286

Kim, Y. S., Ahn, J. Y., You, W. S., & Cho, K. M. (1996). Speed sensorless vector control for brushless DC motor using binary observer. IECON Proceedings (Industrial Electronics Conference), 3, 1746–1751. https://doi.org/10.1109/iecon.1996.570683

Kılıçkır, H. N. (2019). Roketlerin Yönlendirilmesinde Kullanılan Fırçasız Doğru Akım Motorları için Alan Yönlendirme Tabanlı Kanatçık Denetleyici Tasarımı. (Master's Thesis, Pamukkale Üniversitesi Fen Bilimleri Enstitüsü).

Kumar, R., & Padmanaban, S. V. (2006). An Artificial Neural Network based rotor position estimation for sensorless permanent magnet Brushless DC motor drive. IECON Proceedings (Industrial Electronics Conference), 649–654. https://doi.org/10.1109/IECON.2006.347440

L298n dual full-bridge motor driver. (n.d.). Retrieved July 20, 2022, from https://www.pololu.com/product/924/specs

Lee, A. C., Wang, S., & Fan, C. J. (2016). A Current Index Approach to Compensate Commutation Phase Error for Sensorless Brushless DC Motors with Nonideal Back EMF. *IEEE Transactions on Power Electronics*, *31*(6), 4389–4399. https://doi.org/10.1109/TPEL.2015.2468081

Lee, K. W., Kim, D. K., Kim, B. T., & Kwon, B. Il. (2008). A novel starting method of the surface permanent- magnet BLDC motors without position sensor for reciprocating compressor. *IEEE Transactions on Industry Applications*, *44*(1), 85–92. https://doi.org/10.1109/TIA.2007.912734

Lee, W. J., & Sul, S. K. (2006). A new starting method of BLDC motors without position sensor. IEEE Transactions on Industry Applications, 42(6), 1532–1538. https://doi.org/10.1109/TIA.2006.882668

Lee, Y. (2019). A New Method to Minimize Overall Torque Ripple in the Presence of Phase Current Shift Error for Three-Phase BLDC Motor Drive. *Canadian Journal of Electrical and Computer Engineering*, *42*(4), 225–231. https://doi.org/10.1109/CJECE.2019.2907118

Li, H., Zheng, S., & Ren, H. (2017). Self-Correction of Commutation Point for High-Speed Sensorless BLDC Motor with Low Inductance and Nonideal Back EMF. *IEEE Transactions on Power Electronics*, *32*(1), 642–651. https://doi.org/10.1109/TPEL.2016.2524632

Li, Y., Wu, H., Xu, X., Sun, X., & Zhao, J. (2021). Rotor position estimation approaches for sensorless control of permanent magnet traction motor in electric vehicles: A review. World Electric Vehicle Journal, 12(1), 1–26. https://doi.org/10.3390/WEVJ12010009

Montero, E. R., Vogelsberger, M., Ertl, H., & Wolbank, T. (2019). Combination of SVPWM switching states as transient excitation for saliency-based induction machine control. PCIM Europe Conference Proceedings, (May), 1908–1914.

Moreira, J. G. (1996). Indirect Sensing for Rotor Flux Position of Permanent Magnet AC Motors Operationg Over a Wide Speed Range. IEEE Transactions on Industry Applications, 32(6), 1394–1401.

Mousmi, A., Abbou, A., & El Houm, Y. (2017). Trapezoidal control of Brushless DC motor based on DSP F28335. *2017 International Conference on Wireless Technologies, Embedded and Intelligent Systems, WITS 2017*, 17–21. https://doi.org/10.1109/WITS.2017.7934602

Murphy, E., & Slattery, C. (2004). All about direct digital synthesis. Analog Dialogue, 38(3), 8–12. Retrieved from http://www.eecs.yorku.ca/course_archive/2007-08/W/3215/labs documentation/dds.pdf

O'Rourke, C. J., Qasim, M. M., Overlin, M. R., & Kirtley, J. L. (2019). A Geometric Interpretation of Reference Frames and Transformations: Dq0, Clarke, and Park. IEEE Transactions on Energy Conversion, 34(4), 2070–2083. https://doi.org/10.1109/TEC.2019.2941175

Ogasawara, S., & Akagi, H. (1991). An Approach to Position Sensorless Drive for Brushless dc Motors. IEEE Transactions on Industry Applications, 27(5), 928–933. https://doi.org/10.1109/28.90349

PWM Sine Wave Generation. (n.d.). Retrieved November 22, 2022, from https://home.csulb.edu/~hill/ee470/Lab 2d - Sine_Wave_Generator.pdf

Ruangsinchaiwanich, S., Zhu, Z. Q., & Howe, D. (2005). Influence of magnet shape on cogging torque and back-emf waveform in permanent magnet machines. ICEMS 2005: Proceedings of the Eighth International Conference on Electrical Machines and Systems, 1, 284–289. https://doi.org/10.1109/icems.2005.202531

Saha, B., & Singh, B. (2021). Back EMF Observer Based Sensorless BLDC Motor Drive with SEPIC Converter for EV Application. 2021 IEEE 6th International Conference on Computing, Communication and Automation, ICCCA 2021, 94–99. https://doi.org/10.1109/ICCCA52192.2021.9666371

Saied, M. H., Mostafa, M. Z., Abdel- Moneim, T. M., & Yousef, H. A. (2006). On three- phase six-switches voltage source inverter: A 150° conduction mode. IEEE International Symposium on Industrial Electronics, 2, 1504–1509. https://doi.org/10.1109/ISIE.2006.295694

Saribulut, L., Teke, A., & Tümay, M. (2012). Vector-based reference location estimating for space vector modulation technique. Electric Power Systems Research, 86, 51–60. https://doi.org/10.1016/j.epsr.2011.12.004

Senjyu, T., & Uezato, K. (1995). Adjustable speed control of brushless DC motors without position and speed sensors. International IEEE/IAS Conference on Industrial Automation and Control: Emerging Technologies, Proceedings, (5), 160–164. https://doi.org/10.1109/iacet.1995.527556

Shao, J., Nolan, D., Teissier, M., & Swanson, D. (2002). A novel sensorless brushless DC(BLDC) motor drive for automotive fuel pumps. IEEE Workshop on Power Electronics in Transportation, 2002-Janua(6), 53–59. https://doi.org/10.1109/PET.2002.1185550

Shouse, K. R., & Taylor, D. G. (1998). Sensorless velocity control of permanent-magnet synchronous motors. IEEE Transactions on Control Systems Technology, 6(3), 313–324. https://doi.org/10.1109/87.668033

Small high torque motor. (n.d.). Retrieved July 10, 2022, from https://www.magneticinnovations.com/direct-drive-electric-motors/torque-motor-direct-drive/mif-110mm/

Strobl, S. (n.d.). V/f control of an induction machine. Retrieved December 5, 2022, from https://imperix.com/doc/implementation/vf-control-induction-machine

T-motor CubeMars RI50 çerçevesiz Inrunner motor 12V-48V motor BLDC motor düşük dişli tork. (n.d.). Retrieved July 19, 2022, from https://tr.aliexpress.com/i/1005002387271289.html

Tsai, M. F., Quy, T. P., Wu, B. F., & Tseng, C. S. (2011). Model construction and verification of a BLDC motor using MATLAB/SIMULINK and FPGA control. *Proceedings of the 2011 6th IEEE Conference on Industrial Electronics and Applications, ICIEA 2011*, 1797–1802. https://doi.org/10.1109/ICIEA.2011.5975884

Watson, D. (2018). Introduction to arduino nano. Retrieved July 20, 2022, from https://www.theengineeringprojects.com/2018/06/introduction-to-arduino-nano.html

Wang, L., Zhu, Z. Q., Bin, H., & Gong, L. (2021). A Commutation Error Compensation Strategy for High-Speed Brushless DC Drive Based on Adaline Filter. *IEEE Transactions on Industrial Electronics*, *68*(5), 3728–3738. https://doi.org/10.1109/TIE.2020.2984445

Wang, Q., Dong, E., Du, S., Tong, J., Yu, H., & Duan, F. (2022). Mega-Stability and Transient Chaos Analysis of Brushless DC Motor with Winding Heat Loss. 2022 IEEE International Conference on Mechatronics and Automation, ICMA 2022, 1801–1806. Institute of Electrical and Electronics Engineers Inc. https://doi.org/10.1109/ICMA54519.2022.9856249

Xia, C. L. (2012). Permanent Magnet Brushless DC Motor Drives and Controls. In Permanent Magnet Brushless DC Motor Drives and Controls. https://doi.org/10.1002/9781118188347

Yang, L., Zhu, Z. Q., Bin, H., Zhang, Z., & Gong, L. (2021). Virtual Third Harmonic Back EMF-Based Sensorless Drive for High-Speed BLDC Motors Considering Machine Parameter Asymmetries. IEEE Transactions on Industry Applications, 57(1), 306–315. https://doi.org/10.1109/TIA.2020.3033821

Yedamale, P. (2003). Brushless DC (BLDC) Motor Fundamentals. Microchip Technology Inc., (20(1)), 3–15.

Zhou, L., Li, X., Chen, W., & Shi, T. (2021). A Modified Method for Initial Rotor Position Detection of Brushless DC Motor Based on Voltage Vector Injection. 2021 IEEE 4th Student Conference on Electric Machines and Systems, SCEMS 2021 - Proceedings. https://doi.org/10.1109/SCEMS52239.2021.9646113

APPENDICES

APPENDIX A: Open-Loop 120° Commutation Codes

These codes are derived from Adana Alparslan Türkeş Science and Technology University EEE322 Control Methods for Industrial Electrical Machines course material.

```
#define pot A0
//
#define IN1 9
#define IN2 10
#define IN3 11
#define IN4 12
//
#define EN1 2
#define EN2 4
#define EN3 5
#define EN4 7
//
int Delay;
int commutation;
void setup()
{
  pinMode(IN1, OUTPUT);
  pinMode(IN2, OUTPUT);
  pinMode(IN3, OUTPUT);
  pinMode(IN4, OUTPUT);
  //
  pinMode(EN1, OUTPUT);
  pinMode(EN2, OUTPUT);
  pinMode(EN3, OUTPUT);
  pinMode(EN4, OUTPUT);
  //
  pinMode(pot, INPUT);
  //
  digitalWrite(EN1, HIGH);
  digitalWrite(EN2, HIGH);
  digitalWrite(EN3, HIGH);
  digitalWrite(EN4, HIGH);
  //
  digitalWrite(IN1, LOW);
```

```
  digitalWrite(IN2, LOW);
  digitalWrite(IN3, LOW);
  digitalWrite(IN4, LOW);
  //
}
void loop()
{
    Delay = 2 + analogRead(pot) * 10;
    commutate();
}
void commutate()
{
    //1. SECTOR
    digitalWrite(EN1, LOW); digitalWrite(EN2, HIGH); digitalWrite(EN3, HIGH);
                            digitalWrite(IN2, HIGH); digitalWrite(IN3, LOW);
        delayMicroseconds(Delay);
    //2. SECTOR
    digitalWrite(EN1, HIGH); digitalWrite(EN2, LOW); digitalWrite(EN3, HIGH);
    digitalWrite(IN1, HIGH);                         digitalWrite(IN3, LOW);
        delayMicroseconds(Delay);
    //3. SECTOR
    digitalWrite(EN1, HIGH); digitalWrite(EN2, HIGH); digitalWrite(EN3, LOW);
    digitalWrite(IN1, HIGH); digitalWrite(IN2, LOW);
        delayMicroseconds(Delay);
    //4. SECTOR
    digitalWrite(EN1, LOW); digitalWrite(EN2, HIGH); digitalWrite(EN3, HIGH);
                            digitalWrite(IN2, LOW);  digitalWrite(IN3, HIGH);
        delayMicroseconds(Delay);
    //5. SECTOR
    digitalWrite(EN1, HIGH); digitalWrite(EN2, LOW); digitalWrite(EN3, HIGH);
    digitalWrite(IN1, LOW);                          digitalWrite(IN3, HIGH);
        delayMicroseconds(Delay);
    //6. SECTOR
    digitalWrite(EN1, HIGH); digitalWrite(EN2, HIGH); digitalWrite(EN3, LOW);
    digitalWrite(IN1, LOW); digitalWrite(IN2, HIGH);
        delayMicroseconds(Delay);
}
```

APPENDIX B: Open-Loop 150° Commutation Codes

```
#define pot A0
//
#define IN1 9
#define IN2 10
#define IN3 11
#define IN4 12
//
#define EN1 2
#define EN2 4
#define EN3 5
#define EN4 7
//
int Delay;
int commutation;
void setup()
{
  pinMode(IN1, OUTPUT);
  pinMode(IN2, OUTPUT);
  pinMode(IN3, OUTPUT);
  pinMode(IN4, OUTPUT);
  //
  pinMode(EN1, OUTPUT);
  pinMode(EN2, OUTPUT);
  pinMode(EN3, OUTPUT);
  pinMode(EN4, OUTPUT);
  //
  pinMode(pot, INPUT);
  //
  digitalWrite(EN1, HIGH);
  digitalWrite(EN2, HIGH);
  digitalWrite(EN3, HIGH);
  digitalWrite(EN4, HIGH);
  //
  digitalWrite(IN1, LOW);
  digitalWrite(IN2, LOW);
  digitalWrite(IN3, LOW);
  digitalWrite(IN4, LOW);
  //
}
void loop()
{
    Delay = 2 + analogRead(pot) * 10;
    commutate();
}
 void commutate(){
    //1. SECTOR
    digitalWrite(EN1, HIGH); digitalWrite(EN2, HIGH); digitalWrite(EN3, HIGH);
```

```
digitalWrite(IN1, HIGH); digitalWrite(IN2, LOW);  digitalWrite(IN3, HIGH);
  delayMicroseconds(Delay);
//2. SECTOR
digitalWrite(EN1, HIGH); digitalWrite(EN2, HIGH); digitalWrite(EN3, LOW);
digitalWrite(IN1, HIGH); digitalWrite(IN2, LOW);  digitalWrite(IN3, LOW);
  delayMicroseconds(Delay);
//3. SECTOR
digitalWrite(EN1, HIGH); digitalWrite(EN2, HIGH); digitalWrite(EN3, HIGH);
digitalWrite(IN1, HIGH); digitalWrite(IN2, LOW);  digitalWrite(IN3, LOW);
  delayMicroseconds(Delay);
//4. SECTOR
digitalWrite(EN1, HIGH); digitalWrite(EN2, LOW); digitalWrite(EN3, HIGH);
digitalWrite(IN1, HIGH); digitalWrite(IN2, LOW); digitalWrite(IN3, LOW);
  delayMicroseconds(Delay);
//5. SECTOR
digitalWrite(EN1, HIGH); digitalWrite(EN2, HIGH); digitalWrite(EN3, HIGH);
digitalWrite(IN1, HIGH); digitalWrite(IN2, HIGH); digitalWrite(IN3, LOW);
  delayMicroseconds(Delay);
//6. SECTOR
digitalWrite(EN1, LOW); digitalWrite(EN2, HIGH); digitalWrite(EN3, HIGH);
digitalWrite(IN1, LOW); digitalWrite(IN2, HIGH); digitalWrite(IN3, LOW);
  delayMicroseconds(Delay);
//7. SECTOR
digitalWrite(EN1, HIGH); digitalWrite(EN2, HIGH); digitalWrite(EN3, HIGH);
digitalWrite(IN1, LOW);  digitalWrite(IN2, HIGH); digitalWrite(IN3, LOW);
  delayMicroseconds(Delay);
//8. SECTOR
digitalWrite(EN1, HIGH); digitalWrite(EN2, HIGH); digitalWrite(EN3, LOW);
digitalWrite(IN1, LOW);  digitalWrite(IN2, HIGH); digitalWrite(IN3, LOW);
  delayMicroseconds(Delay);
//9. SECTOR
digitalWrite(EN1, HIGH); digitalWrite(EN2, HIGH); digitalWrite(EN3, HIGH);
digitalWrite(IN1, LOW);  digitalWrite(IN2, HIGH); digitalWrite(IN3, HIGH);
  delayMicroseconds(Delay);
//10. SECTOR
digitalWrite(EN1, HIGH); digitalWrite(EN2, LOW); digitalWrite(EN3, HIGH);
digitalWrite(IN1, LOW);  digitalWrite(IN2, LOW); digitalWrite(IN3, HIGH);
  delayMicroseconds(Delay);
//11. SECTOR
digitalWrite(EN1, HIGH); digitalWrite(EN2, HIGH); digitalWrite(EN3, HIGH);
digitalWrite(IN1, LOW);  digitalWrite(IN2, LOW);  digitalWrite(IN3, HIGH);
  delayMicroseconds(Delay);
//12. SECTOR
digitalWrite(EN1, LOW); digitalWrite(EN2, HIGH); digitalWrite(EN3, HIGH);
digitalWrite(IN1, LOW); digitalWrite(IN2, LOW);  digitalWrite(IN3, HIGH);
  delayMicroseconds(Delay);
  }
```

APPENDIX C: Open-Loop 180° Commutation Codes

```
#define pot A0
//
#define IN1 9
#define IN2 10
#define IN3 11
#define IN4 12
//
#define EN1 2
#define EN2 4
#define EN3 5
#define EN4 7
//
int Delay;
int commutation;
void setup()
{
  pinMode(IN1, OUTPUT);
  pinMode(IN2, OUTPUT);
  pinMode(IN3, OUTPUT);
  pinMode(IN4, OUTPUT);
  //
  pinMode(EN1, OUTPUT);
  pinMode(EN2, OUTPUT);
  pinMode(EN3, OUTPUT);
  pinMode(EN4, OUTPUT);
  //
  pinMode(pot, INPUT);
  //
  digitalWrite(EN1, HIGH);
  digitalWrite(EN2, HIGH);
  digitalWrite(EN3, HIGH);
  digitalWrite(EN4, HIGH);
  //
  digitalWrite(IN1, LOW);
  digitalWrite(IN2, LOW);
  digitalWrite(IN3, LOW);
  digitalWrite(IN4, LOW);
  //
}
void loop()
{
    Delay = 2 + analogRead(pot) * 10;
    commutate();
}
 void commutate(){
    digitalWrite(EN1, HIGH); digitalWrite(EN2, HIGH); digitalWrite(EN3, HIGH);
    //1. SECTOR
```

```
digitalWrite(IN1, HIGH); digitalWrite(IN2, HIGH); digitalWrite(IN3, LOW);
  delayMicroseconds(Delay);
//2. SECTOR
digitalWrite(IN1, HIGH); digitalWrite(IN2, LOW); digitalWrite(IN3, LOW);
  delayMicroseconds(Delay);
//3. SECTOR
digitalWrite(IN1, HIGH); digitalWrite(IN2, LOW); digitalWrite(IN3, HIGH);
  delayMicroseconds(Delay);
//4. SECTOR
digitalWrite(IN1, LOW); digitalWrite(IN2, LOW); digitalWrite(IN3, HIGH);
  delayMicroseconds(Delay);
//5. SECTOR
digitalWrite(IN1, LOW); digitalWrite(IN2, HIGH); digitalWrite(IN3, HIGH);
  delayMicroseconds(Delay);
//6. SECTOR
digitalWrite(IN1, LOW); digitalWrite(IN2, HIGH); digitalWrite(IN3, LOW);
  delayMicroseconds(Delay);
  }
```